Matrix Biology 141 (2025) 82–100

Contents lists available at ScienceDirect

Matrix Biology

journal homepage: www.elsevier.com/locate/matbio

# Biomechanical and compositional basement membrane defects due to a *Col4a1* mutation affect cardiac morphology and function

Erin Boland [a,*], Anna Hoyle [d], Olivia Robertson-Gray [a], William Fuller [a], Joe Swift [e], Marco Cantini [b], Matthew Walker [b], Eline Huethorst [a], Eilidh MacDonald [a], Christoper Loughrey [a], Manuel Salmeron-Sanchez [b], Godfrey L. Smith [a], Fabio Quondamatteo [c], Tom Van Agtmael [a,*]

[a] University of Glasgow, School of Cardiovascular and Metabolic Health, Glasgow, United Kingdom
[b] University of Glasgow, School of Engineering, Glasgow, United Kingdom
[c] Tissue Engineering Research Group, Department of Anatomy and Regenerative Medicine, Royal College of Surgeons in Ireland, Dublin, Ireland
[d] Kennedy Institute of Rheumatology, University of Oxford, Oxford, United Kingdom
[e] Manchester Cell-Matrix Centre, The University of Manchester, Manchester, United Kingdom

ARTICLE INFO

*Keywords:*
Basement membrane
Cardiac function
Cardiomyopathy
Extracellular matrix
Fibrosis
Collagen IV
Gould syndrome

ABSTRACT

Collagen IV is a major constituent of basement membranes and mutations in the genes *COL4A1* and *COL4A2* present clinically as a variable, multi-system disorder called COL4A1 (Gould) syndrome. Evidence from case reports supports a cardiac component to this disease, but the phenotypic and functional implications affecting the heart, their progression and underlying mechanisms all remain poorly characterised. Indeed, the role of the basement membrane (BM) in adult cardiac disease remains underexplored. We set out to address these knowledge gaps by combining in-depth phenotypic and molecular analyses of a *Col4a1* mutation on cardiac biology in a murine model (*Col4a1*$^{+/svc}$) of Gould Syndrome. This revealed morphological cardiac defects including cardiomyocyte hypertrophy with myocardial and vascular fibrotic remodelling that impaired cardiac function. The *Col4a1* mutation causes systolic and diastolic dysfunction with reduced left ventricular developed pressure. Mechanistically, we show these defects are due to secretion of mutant protein and BM defects rather than collagen misfolding and proteotoxic stress. The BM defects lead to a pro-fibrotic state with increased fibrillar collagen deposition, cardiac stiffness, and ECM compositional defects. These are accompanied by altered regulation of pathways involved in sarcomere formation, sarcolemma stability and cardiomyocyte metabolism, establishing a molecular signature of COL4A1-related cardiac disease. Intriguingly, aspects of this molecular signature including cardiac metabolic pathways, regulation of cardiac muscle contraction and BM component expression, are shared with common cardiomyopathies such as coronary micro-embolism, and dilated, ischemic and hypertrophic obstructive cardiomyopathies. By defining the molecular and phenotypic cardiac components of Gould syndrome these data show that the BM is essential for maintaining systolic and diastolic function and that alterations to the BM leads to a fibrotic response. These data increase insight into the role of the basement membrane and collagen IV in cardiac biology, and highlights mechanisms shared between Gould syndrome and common adult cardiac disease.

## Introduction

Basement membranes (BMs) are extracellular matrix (ECM) structures that anchor cells to the surrounding interstitial matrix, and influence cell differentiation, signalling, and migration [1,2]. Within the heart BMs surround cardiomyocytes, and the vascular BMs separates

*Abbreviations:* AFM, atomic force microscopy; BM, basement membrane; CME, coronary microembolism; CSA, cross-sectional area; ECM, extracellular matrix; ER, endoplasmic reticulum; DCM, dilated cardiomyopathy; HCM, hypertrophic cardiomyopathy; ICM, ischemic cardiomyopathy; IVS, interventricular septum; LV, left ventricle; RV, right ventricle; SVC, small with vacuolar cataract (*Col4a1*$^{+/svc}$); WT, wild type.

* Corresponding authors.
*E-mail addresses:* Erin.Boland@glasgow.ac.uk (E. Boland), Tom.VanAgtmael@glasgow.ac.uk (T. Van Agtmael).

https://doi.org/10.1016/j.matbio.2025.09.003
Received 1 August 2025; Received in revised form 29 August 2025; Accepted 11 September 2025
Available online 12 September 2025

endothelial and vascular smooth muscle cells [3]. Little is understood about how BMs in the heart regulate cardiac function and the impact of mutations in BM components thereon [3].

Collagen IV is a heterotrimeric protein encoded by six genes, *COL4A1–6*, encoding α chains α1-α6(IV). Three collagen IV α chains interact in the endoplasmic reticulum (ER) to produce three heterotrimeric protomers; α1.α1.α2(IV), α3.α4.α5 (IV), and α5.α5.α6 (IV) which when secreted form a three-dimensional lattice style network in the BM [4,5]. The original description of phenotypes in mice with *Col4a1* mutations, including *Col4a1*$^{+/svc}$ (small with vacuolar cataract), led to the identification of *COL4A1* and *COL4A2* mutations in patients and the description of a complex multi-systemic syndrome, called Gould Syndrome (aka COL4A1/2-related Syndrome) that encompasses vascular, ocular, renal and muscular defects [6]. The cerebrovascular phenotypes have received most attention and *COL4A1/2* variants are now recognised as major factors in sporadic and genetic forms of stroke and small vessel disease [4,7–16]. Missense mutations affecting the Gly residue of the Gly-Xaa-Yaa motif of the central collagenous domain account for ~70 % *COL4A1* and *COL4A2* mutations in Gould Syndrome [17]. The development of Gould Syndrome and the severity of the phenotypes is dependent on the type of mutation and its location within the α chain [6,18]. Drosophila [19] and murine models effectively recapitulate this phenotypic heterogeneity as the *Col4a1*$^{+/svc}$ (G1064D) and *Col4a1*$^{+/bru}$ (G627W) mouse lines have more severe disease progression compared to *Col4a1*$^{+/raw}$ mice (K950E) [13]. The *Col4a1*$^{+/svc}$ (G1064D) mutation affects a glycine residue three repeats from a two amino acid interruption in the Gly-Xaa-Yaa repeat [6] and maps close to a putative HSP47 binding site [20]. Combined, these data underscore the power of these mouse models to uncover molecular disease mechanisms and phenotypes in the human disease.

Cardiac defects have been reported in patients with *COL4A1* or *COL4A2* mutations. Case studies reported mitral valve defects affecting outflow from the left ventricle [21], dilation of the right ventricle, hypoplasia of the left ventricle, ventricular septal defect and hypoplastic aortic arch [22]. Reported functional defects include supraventricular arrhythmia [10,23] in HANAC Syndrome, a clinical sub-entity of Gould Syndrome, and depressed LV systolic function accompanied with severe respiratory distress and bradycardia in a single neonate [24]. In addition to these missense variants, deletions of regions of chromosome 13 that encompass *COL4A1* and *COL4A2* have been implicated in congenital heart defects including double outlet right ventricle, pulmonary stenosis, and both atrial and ventricular septal defects [25,26]. All these studies were limited in scope, did not provide an in-depth analysis and were often single case reports. Thus, the cardiac component of Gould Syndrome remains poorly defined.

Genetic studies further support a role for collagen IV in cardiac disease in the general population, identifying *COL4A1* and *COL4A2* variants as risk factors for myocardial infarction, arterial stiffness, familial coronary artery dissection, and cardiovascular mortality [27–31], while elevated α1(IV) plasma levels have been identified as a biomarker for atrial fibrillation [32]. Altogether, this supports the concept that *COL4A1/COL4A2* mutations can affect cardiac morphology and function.

Mouse models with *Col4a1* mutations, such as *Col4a1*$^{+/svc}$, faithfully recapitulate Gould Syndrome [6,33–36]. *COL4A1/2* mutations can cause disease either due to mutant protein incorporation in the BM, reduced collagen IV levels in the BM, and/or retention of mutant protein in the endoplasmic reticulum (ER) resulting in ER stress [7,34,37,38]. Unabated ER stress can be pathogenic, and collagen IV ER retention was associated with disease in a family carrying a *COL4A2* mutation, while in mice it was associated with intracerebral haemorrhage severity [33, 39]. These upstream mechanisms are not mutually exclusive, and we previously showed evidence of cell specific mechanisms for the same mutation [37,40] Absence of collagen IV in mice leads to rudimentary disorganised BMs that no longer fully surround cardiomyocytes, and embryonic lethality with extensive cardiac defects [41].

BM components interact dynamically with mechanosensitive cell membrane receptors including integrins, dystroglycan and discoidin domain receptors with specific isoforms of these receptors being expressed throughout the myocardium [42–47]. The transduction of biomechanical changes via the ECM and cell membrane receptors results in intracellular changes critical for cardiomyocyte function but that can also drive pathological changes [48].

Here, we investigated the impact of *Col4a1* mutations on cardiac morphology and function to identify key underlying pathomolecular pathways. This revealed that the *Col4a1*$^{+/svc}$ mutation causes cardiac pathology and contractile dysfunction via biomechanical and compositional basement membrane defects. Proteomic analysis coupled with analysis of proteomic datasets of mouse and human heart disease, including sporadic cardiomyopathy and coronary embolism, revealed a shared molecular signature encompassing mitochondrial function, cardiac contractility and metabolic processes. These data underscore the role of basement membranes in heart physiology and pathophysiology.

## Results

### *Col4a1*$^{+/svc}$ *mice develop age dependent cardiac phenotype with increased fibrosis and passive myocardial tissue stiffness*

To shed light on the cardiac component in Gould Syndrome and the impact of collagen IV mutations on cardiac morphology and pathophysiology, we carried out a histopathological analysis of *Col4a1*$^{+/svc}$ hearts including H&E staining for general morphological defects and picrosirius red staining to determine if there was a fibrotic response to the mutant Col4a1 protein. This revealed increased collagen deposition in *Col4a1*$^{+/svc}$ intramyocardial coronary vessels that was most notable around the vascular adventitia and indicate the development of perivascular fibrosis (Fig. 1**A**). In addition, infiltration of collagen fibres within the tunica media occurred in mutant vessels, disrupting smooth muscle cell layer organisation (Fig. 1**A**). While in 3-month-old mice this fibrosis was primarily localised to the coronary vasculature, regions of fibrosis within all regions of myocardium were noticed in a subset of older *Col4a1*$^{+/svc}$ mice (Fig. 1**B**).

Haematoxylin and eosin (H&E) staining and analysis revealed normal overall cardiac morphology at 3-months old. However, the presence of invaginations, called clefts, was observed in the myocardium. These occur between individual cardiomyocytes and analysis of 12-month-old mutants revealed this pathology progressed with age most prominently within the left ventricle (Fig. 1**C-D**). 3-month-old *Col4a1*$^{+/SVC}$ mice showed no alterations in heart weight (Supplemental **Fig. 1A-C**).

To determine if this pathology alters the biomechanical properties of the myocardium, atomic force microscopy, was performed on heart sections to measure elasticity and stiffness of left and right myocardial tissue. This technique involves precise surface indentations of the material of interest and has been previously used to establish stiffness and elasticity in myocardial tissue and cardiomyocyte preparations [49–51]. This demonstrated a significantly increased Young's modulus in the left and right ventricular myocardium of *Col4a1*$^{+/svc}$ mice (Fig. 1**E-F**) with a 2.7-fold (LV, WT - 4.46 kPa ± 9.6, *Col4a1*$^{+/svc}$ −15.2 kPa ± 18.2) and 2.2-fold (RV, WT - 15.8 kPa ± 31.8, *Col4a1*$^{+/svc}$ - 41.02 kPa ± 61.54) increase, respectively ($p < 0.0001$, unpaired two-tailed *t*-test, $n = 3$). These data reveal that *Col4a1* mutations cause progressive cardiac pathology with increased passive myocardial stiffness and fibrosis.

### *Col4a1*$^{+/svc}$ *mice develop right ventricular cardiomyocyte hypertrophy*

The density of the capillary network is important to provide adequate perfusion of the cardiomyocyte to prevent hypoxia and deliver metabolic substrates. *Col4a1* mutations have been associated with angiogenesis defects in other tissues [52,53]. Thus, to establish if changes in capillary density was a phenotypic feature in 12-month-old

*Col4a1*$^{+/svc}$ mice, we stained endothelial cells with Isolectin B4 (Fig. 2**A**). This revealed no significant differences in capillary density (left ventricle $p = 0.657$, interventricular septum $p = 0.293$, right ventricle $p = 0.219$) (Fig. 2**B**).

To investigate if *Col4a1* mutations impact cardiomyocyte size we performed wheat germ agglutinin staining, which stains the sarcolemma (Fig. 2**C**), to calculate cardiomyocyte cross-sectional area (CSA). This showed in *Col4a1*$^{+/svc}$ mice that WGA positive regions were

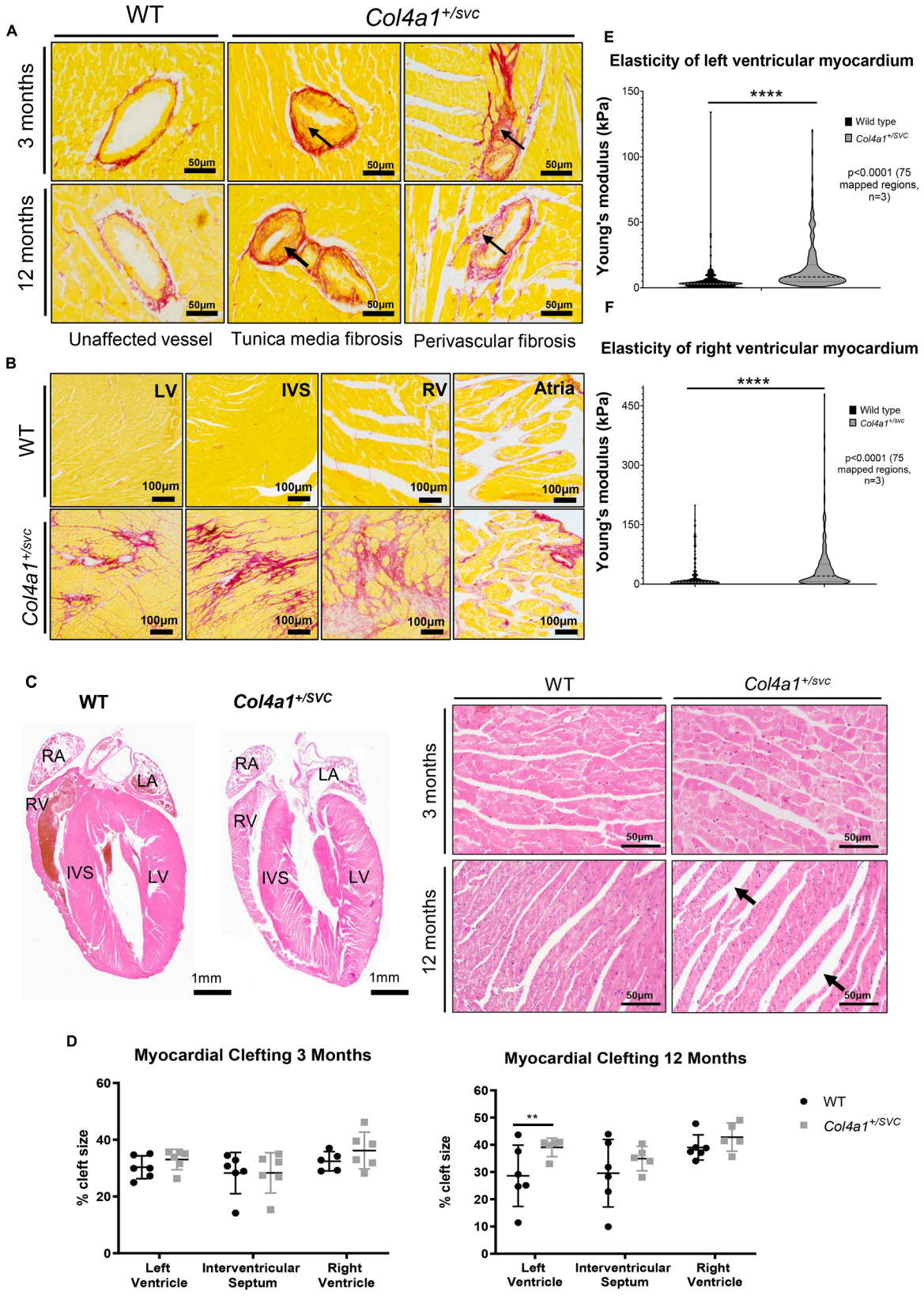


*(caption on next page)*

**Fig. 1. Characterising cardiac morphology of *Col4a1*$^{+/svc}$ mice. (A)** Picrosirius red stained sections of mutant coronary vasculature show increased collagen deposition within the tunica media and perivascular fibrosis (arrows). One 12-month-old *Col4a1*$^{+/svc}$ animal also revealed extensive myocardial fibrosis within the right ventricle and fibrosis and occlusion of the right coronary artery. **(B)** Areas of focal myocardial fibrosis present surrounding atrial cardiomyocytes, interventricular septum (IVS), left ventricle (LV) and right ventricle (RV) within a severely affected *Col4a1*$^{+/svc}$ 12-month-old mouse. **(C)** Haematoxylin and eosin staining shows an increase in the presence of myocardial cleft size within the left ventricular myocardium of 12- month-old mutants compared to 3-month-old mutants (black arrows), highlighting disease progression with age (WT = 28.62 %, *Col4a1*$^{+/svc}$ = 39.08 % $p = 0.041$. Interventricular Septum - WT = 29.59 %, *Col4a1*$^{+/svc}$ = 34.94 % $p = 0.281$. Right Ventricle - WT = 39.05 %, *Col4a1*$^{+/svc}$ = 42.85 % $p = 0.442$. Unpaired two-tailed *t*-tests, WT = 6, *Col4a1*$^{+/svc}$ = 5). **(D)** Cleft size analysis the left ventricle (LV), interventricular septum (IVS), and right ventricle (RV) of 3 and 12-month-old mice revealed an increase in myocardial spacing within the LV of older mutants. **(E)** *Col4a1*$^{+/svc}$ mice have significantly decreased elasticity of the left and **(F)** right ventricular myocardium. Young's modulus analysis of left and right ventricular myocardium revealed a statistically significant increase in the stiffness of the myocardial tissue in both regions in *Col4a1*$^{+/svc}$ hearts compared to WT controls (Left ventricular myocardium WT = 5564 kPa v *Col4a1*$^{+/svc}$ = 15,200 kPa, $p < 0.0001$. Right ventricular myocardium WT = 19,116 kPa v *Col4a1*$^{+/svc}$ = 41,771 kPa $p < 0.0001$, unpaired two-tailed *t*-test of 75 mapped data points per animal, per region, $n = 3$).

inconsistent, and not all cardiomyocytes were fully surrounded (Fig. 2C). CSA analysis of intact cardiomyocytes of 3-month-old animals revealed no evidence of hypertrophy, but 12-month-old *Col4a1*$^{+/SVC}$ mice had hypertrophic cardiomyocytes (1.56-fold increase) in the right ventricle (Fig. 2D). This indicates a hypertrophic response accompanying the fibrosis. Coupled with the lack of increase in capillary density,

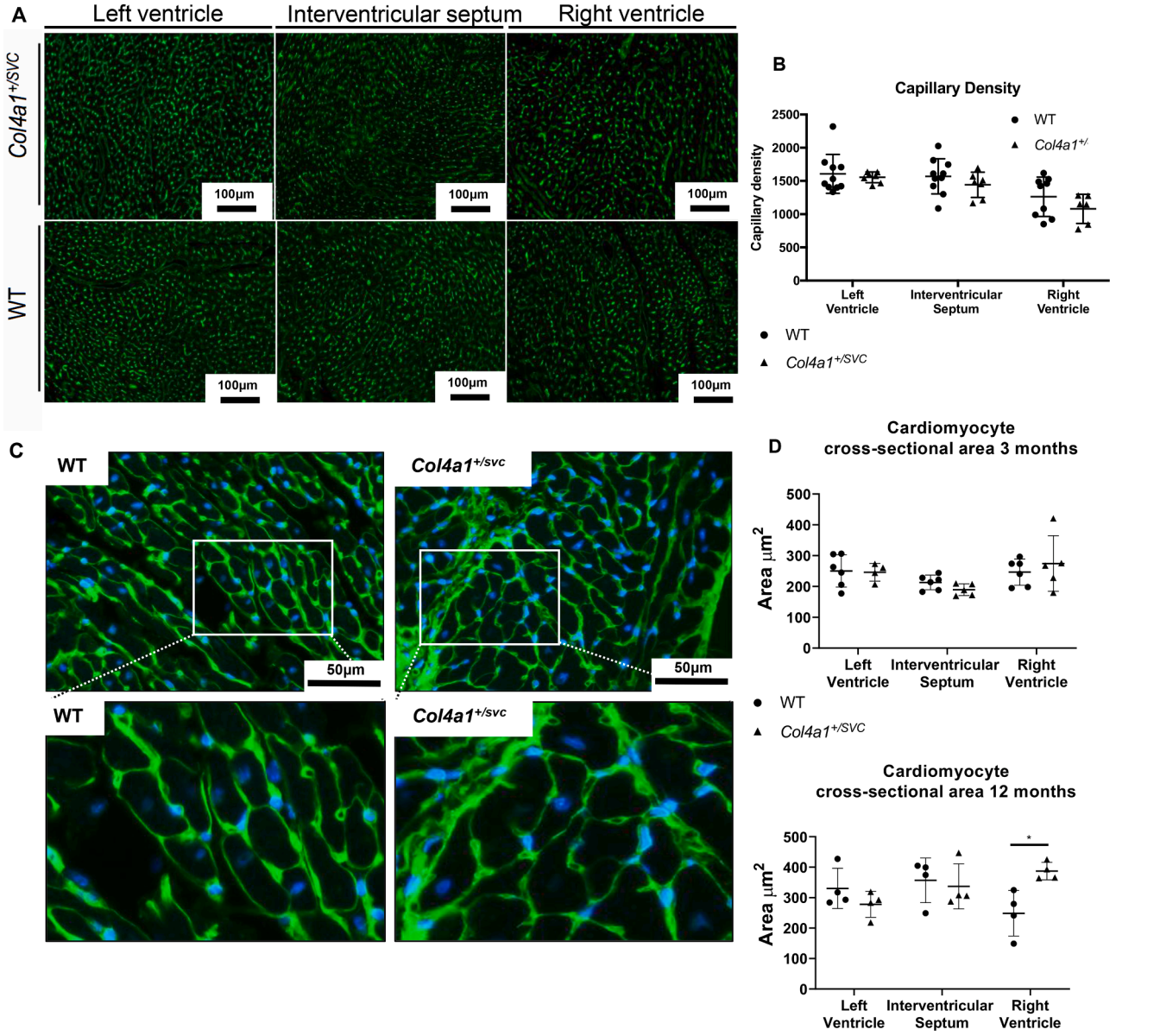


**Fig. 2. Assessment of myocardial vascularisation and hypertrophy. (A) Capillary density quantification of *Col4a1*$^{+/svc}$ myocardium.** Myocardial capillaries were visualised by Isolectin B4 immunostaining for endothelial cells. The number of capillaries per region was quantified however not statistically significant difference was detected in capillary density in any region of myocardium (left ventricle $p = 0.657$, interventricular septum $p = 0.293$, right ventricle $p = 0.219$, WT $n = 9$, *Col4a1*$^{+/svc}$ $n = 6$). Cardiomyocyte cross-sectional area (CSA) in *Col4a1*$^{+/svc}$ hearts. **(B)** Wheat germ agglutinin staining of the right ventricle in WT & *Col4a1*$^{+/svc}$ mice (green). **(C)** CSA analysis of the left ventricle, right ventricle and interventricular septum revealed a significant increase in the CSA of cardiomyocytes only within the right ventricle (WT = 248.7 µm, *Col4a1*$^{+/svc}$ = 387.2 µm $p = 0.5531$, unpaired two-tailed *t*-tests, $n = 4$).

this points towards potential inadequate perfusion of hypertrophic cardiomyocytes.

### *Col4a1*$^{+/svc}$ *mice display impaired left ventricular contractile capacity*

To assess the extent to which the *Col4a1* cardiomyopathy affects cardiac function we performed Langendorff isolated heart perfusion experiments. In 3-month-old mice this revealed maximal pressure (Pmax) was significantly decreased, which is indicative of systolic dysfunction and a reduced contractile capability of the left ventricle (Fig. 3**A**). Calculation of left ventricular developed pressure (LVDP), a commonly used measured of LV performance, was reduced in *Col4a1*$^{+/svc}$ mice with a 54 % reduction in contractile function ($p = 0.0004$ unpaired two-tailed *t*-test). Calculation of the maximum rates of relaxation and contraction (dP/dtmin, dP/dtmax) also uncovered a significant 44 % and 48 % reduction in the rate of relaxation and contraction of the left ventricle respectively ($p = 0.0047$ and $p = 0.0014$ respectively, unpaired two tailed *t*-test) (Fig. 3**A**).

In *Col4a1*$^{+/svc}$ hearts, dP/dtmin (derivative of time to minimum pressure) progressively declined with increasing stimulation rate (Fig. 3**B**). This diminished response reflected poorer diastolic function compared to WT hearts (**Supplementary Table 1.1**). In addition to the reduced dP/dtmin response, the rate of contraction (dP/dtmax) and LV developed pressure were significantly decreased in mutant hearts as stimulation rate increased (**Supplementary Fig.3, Supplementary Tables 1.2 & 1.3**). These data together indicate both systolic and diastolic dysfunction in *Col4a1*$^{+/svc}$ hearts.

### *Col4a1*$^{+/svc}$ *hearts display no change in the localisation of key basement membrane components*

Work by us and others revealed reduced secretion of collagen IV due to glycine mutations [4,9,18,35,54], and that in kidney reduced BM deposition can lead to fibrotic ECM deposition [55]. To determine if altered levels and/or mislocalisation of key BM components was a feature of *Col4a1*$^{+/svc}$ myocardial tissue, we performed immunohistochemistry on 3 and 12-month-old hearts. Surprisingly, and in contrast to for example kidney, overall α1(IV) expression was not significantly altered [35] (Fig. 4**A**) (LV $p = 0.4248$ −13.95 %, IVS $p = 0.4000$ −15.79 %, and RV $p = 0.0703$ −21.87 % unpaired two-tailed *t*-test). Data from drosophila and *Col4a1*$^{+/svc}$ kidney support that perlecan levels can be influenced by collagen IV BM deposition [37,56]. However, perlecan levels were not reduced in the cardiac BM (Fig. 4**B**) (LV $p = 0.5031$, IVS $p = 0.9006$, RV $p = 0.9593$ unpaired two-tailed *t*-tests). PAS staining to investigate if the fibrosis in *Col4a1*$^{+/svc}$ hearts was associated with gross BM zone defects showed overt interruptions and reduced staining in mutant hearts, indicating BM defects and a fibrotic ECM due to the *Col4a1* mutation (Fig. 4**C**). We complemented this analysis by determining levels of *Col4a1, Col4a2, Lama2, Lama4, Lama5, Nid1 and Nid2* mRNA. *Col4a1* was not altered in 3 or 12-month-old *Col4a1*$^{+/svc}$ mice. However, *Col4a2* levels significantly increased in the mutant hearts with age (*Col4a2p* = 0.05 3-month-old WT vs. 12-month-old *Col4a1*$^{+/svc}$, $p = 0.0011$ 3-month-old *Col4a1*$^{+/svc}$ vs. 12-month-old *Col4a1*$^{+/svc}$, Kruskal-Wallis with Dunn's multiple comparisons test) (Fig. 4**D**). No significant differences were observed for laminin or nidogen.

### *Col4a1*$^{+/svc}$ *mice display increased expression of ER-stress markers with disease progression*

Collagen misfolding due to glycine mutations with subsequent ER stress has emerged as a convergent mechanism for diseases associated with several collagen types including collagens I, III, IV, and X [9,57–60]. It is well documented that ageing reduces the capacity of cells to maintain proteostasis. This made us question whether age-related ER stress can occur in Gould Syndrome and thus be associated with the increasing severity of cardiac histological phenotypes with age. However, only Grp94 protein levels were significantly elevated ($p = 0.0006$, unpaired two-tailed *t*-test), while the ratio of p-Eif2α to total Eif2α was significantly decreased (Fig. 5**A-C**). This suggest that in 12-month-old mice activation of the PERK arm of the UPR is supressed (PERK phosphorylates eIF2α; $p = 0.0049$, unpaired two-tailed *t*-test). Combined this does not present a clear sign of ER stress with UPR activation but it does point towards potential dysregulated ER proteostasis with age. Upregulation of the apoptotic marker *Caspase3* was observed in younger *Col4a1*$^{+/svc}$ animals (Fig. 5**D-E**).

### *Col4a1*$^{+/svc}$ *cardiac disease includes dysregulated cell-matrix adhesion*

ECM homeostasis is determined by a balance between ECM deposition and turnover and degradation, which is mediated by proteases and their inhibitors. Recent in vitro evidence has indicated elevated MMP levels due to *COL4A1* mutations [61]. Analysis of mRNA levels of a subset of proteins involved in matrix turnover and degradation, *Mmp14, Mmp2, Mmp9, Timp2* and *Adam12,* revealed significant increases in ECM proteinases in mutants at 3 months which declines in older mice (Fig. 6**A**). This is accompanied by altered mRNA levels of proteins involved in cell-cell and cell-ECM adhesion and signalling such as *αPax, Icam-1,* and *Itga2.*

Altogether, expression analysis of 50 candidate genes previously implicated in cardiovascular disorders revealed a global shift in expression coinciding with the onset of functional impairment in 3-month-old *Col4a1*$^{+/svc}$ mice (Fig. 6**A**). Gene Ontology analysis of associated biological process further revealed the key pathways in which these candidate genes are involved and among the top 20 significant pathways were regulation of cell adhesion, migration and motility, heart and circulatory system development, cell-matrix adhesion (Fig. 6**B**). Tube and branching epithelial morphology was also identified highlighting the role of BM genes in angiogenic processes (Fig. 6**C**).

### *Basement membrane composition and ECM-cell interaction in Col4a1*$^{+/svc}$

Our candidate mRNA analysis provided support that extensive changes in gene expression occur in response to the *Col4a1* mutation. To create holistic insight into underlying molecular pathways, including ECM composition and cellular responses, we performed proteomic analysis on ECM-enriched and cellular fraction of hearts from 3-month-old *Col4a1*$^{+/svc}$ mice and wild type littermates. Proteins in the matrix enriched fractions were normalised to matrisomal protein abundance and classified using MatrisomeDB classifications [62] (**Supplementary figure 5**). Complete lists of proteins identified in intracellular and extracellular fractions are provided **in Supplementary Tables 6.1 & 6.2.**

Mutant hearts showed overall reduced levels of collagens but higher levels of ECM regulators (Fig. 7**A**), such as Cathepsin B and Transglutaminase 2 that function in ECM remodelling and degradation, and progression of cardiovascular diseases [63–66]. Many BM components were increased in mutant hearts. Increased levels of α1(IV) and α2(IV) in ECM enriched fractions compared (α1(IV): fold change 1.136, $p = 0.026$; α2(IV) fold change 0.751, $p = 0.046$) support secretion of mutant collagen IV. This is combined with increases for some laminins (Lama2: fold change 0.176, $p = 0.00004$; Lama4 fold change 0.631, $p = 0.00007$), nidogen (Nid2 fold change 0.609, $p = 0.00024$) and perlecan (Hspg2, fold change 0.370, $p = 2.45579\text{E-}21$). In contrast collagen VI alpha chain 3 (fold change −0.129, $p = 0.00007$) and alpha 6 (fold change −0.293, $p = 0.00338$) showed reduced levels (Fig. 7**B**), while fibrillar collagens e.g. α1(I) and α2(I) were not altered.

*Col4a1*$^{+/svc}$ hearts displayed alterations in ECM-cell and cell-cell binding (Fig. 7**C**). This is illustrated by increased levels of four-and-a-half LIM domains 2 protein (Fhl2) ($p = 1.51\text{E}^{-15}$, fold change 0.568), vinculin ($p = 1.66279^{\text{E-}17}$, fold change −0.318), which links the cytoskeleton to adherens junctions and focal adhesions to organise

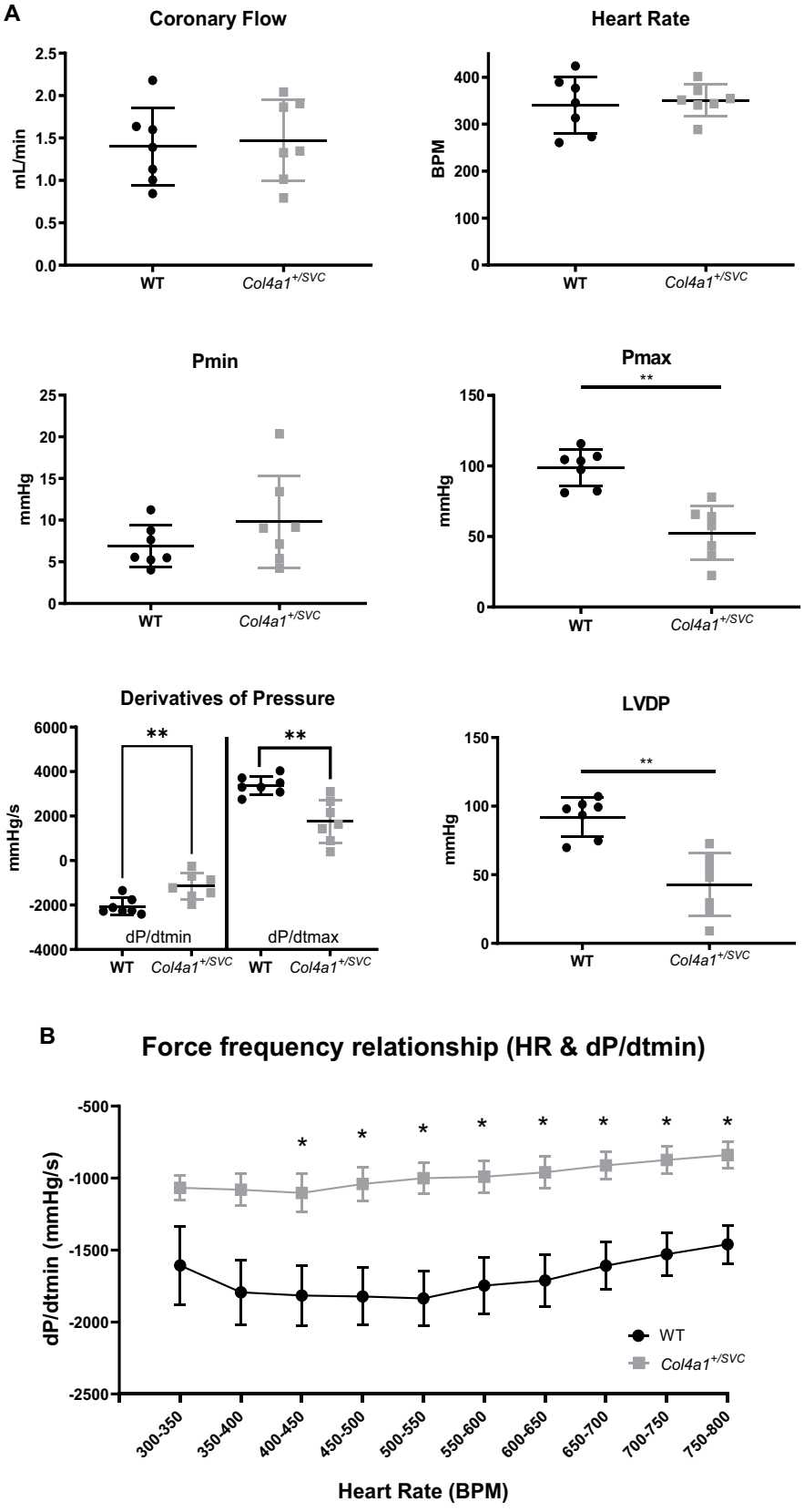


**Fig. 3. Characterisation of *Col4a1*$^{+/svc}$ *ex vivo cardiac function.*** (**A**) Baseline cardiac function of WT and *Col4a1*$^{+/svc}$ mice as determined by Langendorff isolated heart perfusion. *Ex vivo* analysis revealed no significant difference in coronary flow, heart rate, or end diastolic pressure (Pmin) between both groups. Significant differences were observed in the end systolic pressure (Pmax), rate of diastole – time to reach Pmin (dP/dtmin), rate of systole – time to reach Pmax (dP/dtmax) and left ventricular developed pressure, LVDP (Pmax – Pmin) $n = 7$. (**B**) Diastolic function was reduced over a range of stimulation frequencies in *Col4a1*$^{+/svc}$ hearts. The

relationship between dP/dtmin with increasing stimulation rate (300–800 BPM) revealed consistently reduced rate of relaxation irrespective of stimulation rate (error bars representative of SEM, WT $n = 8$ and *Col4a1*$^{+/svc}$ $n = 6$).

cardiomyocyte myofibrils and gap junctions [67,68], and Plakoglobin ($p = 0.00379$, fold change −0.169), a component of cardiomyocyte desmosome and adherens junctions (Fig. 8& 9).

### *Altered cardiomyocyte morphology and repair, and sarcomere formation in Col4a1*$^{+/SVC}$ *hearts*

Cardiomyocyte membrane integrity and sarcolemma micro-architecture are critical to cardiac function. Upregulated proteins involved in caveolae formation (Fig. 9), including the proteins EH-domain containing 2 (Ehd2) and Polymerase I and transcript release factor (Ptrf, also known as Cavin-1) support alterations in membrane morphological features. Higher levels of Mitsugumin 53, which recruits small vesicles to sites of membrane injury [69] provides evidence of sarcolemma repair and damaged cardiomyocytes in *Col4a1*$^{+/svc}$ hearts.

Sarcomeres are critical for cardiac contraction and function, and lower levels of the sarcomere proteins titin (Ttn, $p = 0.00128$, fold change −0.857) and desmin (Des; $p = 0.0008$, fold change −0.226) levels in *Col4a1*$^{+/svc}$ could reflect a reduction in sarcomere number and/or formation (Fig. 9). Titin contributes to passive myocardial stiffness in response to mechanical strain [70] and desmin is the major intermediate filament component in striated muscle cells that links sarcomeres to the cytoskeleton, intercalated disks, and organelles [71]. Similar to *Col4a1*$^{+/svc}$ hearts, *Des*$^{-/-}$ deficiency induces cardiac hypertrophy, systolic dysfunction and increased fibrotic and calcified deposits [72,73]. The lower levels of Ttn and Des are accompanied by upregulation of proteins involved in cardiomyocyte sarcomere assembly and function (Fig. 9) including Myosin Light Chain 2 (*Myl2*) and 4 (*Myl4*), Titin-cap (*Tcap*) (Myl2 $p = 0.000319$, 0.829-fold change, Myl4 $p = 0.00399$, 1.077-fold change, Tcap $p = 0.00015$, 0.493-fold change), Myomesin 2 (*Myom2*) and Myozenin 2 (*Myoz2*) (*Myom2p* = 9.89069E$^{-20}$, 0.282-fold change, *Myoz2p* = 0.0209, 0.199-fold change). Overall, this may point to the activation of programmes aimed at repairing sarcomere damage and loss.

### *Modulators of the cardiac hypertrophy/injury response are altered*

Our staining indicated hypertrophy in *Col4a1*$^{+/svc}$ hearts. Signal transducers and transcriptional activation protein 1 (*Stat1*) regulates cell differentiation and apoptosis [74] and *Stat1*$^{-/-}$ mice develop pressure overload induced hypertrophic cardiomyopathy with pro-fibrotic signalling and impaired mitochondrial function [75]. Focal adhesion kinase (Fak) regulates cell-ECM adhesion and migration [76], activates Stat1 in cell migration with Stat1 depletion causing enhanced cell adhesion [77] and Fak inactivation promotes cardiac hypertrophy [78]. Stat1 was one of the most downregulated proteins in *Col4a1*$^{+/svc}$ ($p = 0.023$, fold change −1.523) (Fig. 8) and while Fak levels were not altered in *Col4a1*$^{+/svc}$, Talin 1 (Tln1) a mechanosensitive protein that is recruited to focal adhesions by Fak [79], was significantly downregulated ($p = 6.99$E$^{-06}$, fold change −0.219). This suggests altered focal adhesion dynamics in cardiac hypertrophy of *Col4a1* mutant mice.

### *Cardiac metabolism is perturbed in Col4a1*$^{+/SVC}$ *mice*

Proteomic analysis of *Col4a1*$^{+/svc}$ hearts indicates dysregulated cardiac metabolism (Fig. 7**C**). Fatty acid beta oxidation and ATP metabolic processes via the TCA cycle appeared downregulated as levels of enzymes in each of these pathways were lower. This included: Electron-transfer-flavoprotein, alpha subunit (Efta, $p = 0.00028$, fold change −0.48) and Electron transfer flavoprotein dehydrogenase (Etfgh, $p = 0.000122$, fold change −0.646) for fatty acid beta oxidation; Succinyl-CoA ligase (GDP-forming) L subunit alpha (Suclg1 $p = 0.0189$, fold change −0.464) and Succinyl-CoA ligase (ADP-forming) subunit beta, mitochondrial (Sucla2, $p = 0.0049$, fold change −0.301) for TCA cycle; subunits of respiratory complex 1, NADH dehydrogenase, (Ndufs1 $p = 0.00231$, fold change −0.139. Nudfa8 $p = 0.008$, fold change −0.459. Ndufa7 $p = 0.019$, fold change −0.171) and subunits of the key enzyme in cellular respiration, ATP synthase (Atp5c1 $p = 0.0309$, fold change −0.984. Atp5f1 $p = 0.0000252$, fold change −0.362. Atp5pb $p = 0.0189$, fold change −0.386). This indicates metabolic shift from fatty acid beta oxidation to less efficient glycolysis (Fig. 8–9).

### *Shared proteomic signature of Col4a1*$^{+/SVC}$ *cardiac proteome with common cardiac pathologies*

To provide further insight into the nature of the cardiac disease and relevance of collagen IV to human cardiac disease in the general population, we cross-referenced differentially expressed proteins with other published proteomic datasets combining human and murine studies of dilated/hypertrophic/ischemic/obstructive cardiomyopathies and coronary micro-embolism [80–83]. GEO biological process analysis revealed that the majority of the shared DEP's between dilated cardiomyopathy and ischemic cardiomyopathy and *Col4a1*$^{+/svc}$ are involved in fatty acid beta-oxidation using acyl-CoA dehydrogenase and the respiratory electron transport chain including electron transfer flavoprotein dehydrogenase (Etfdh), electron transfer flavoprotein subunit alpha (Etfa) and cytochrome-C oxidase subunit 5B (Cox5b). All biological processes with an FDR $p < 0.05$ with the exception of muscle organ development ($p = 2.88$E$^{-05}$) were related to cardiac metabolic activity highlighting the similarity of perturbed metabolic processes between DCM, ICM and *Col4a1*$^{+/svc}$ hearts (Fig. 10**B**) and the impact of ECM alteration thereon.

The greatest overlap between data sets was with a murine model of coronary micro-embolism (CME) (Fig. 10**C&D**). GO analysis of shared DEP's alpha actinin 1 (Actn1), filamin A (Flna), and Myomesin-2 (Myom2) points to biological function of regulation of cardiac muscle contraction. Plakoglobin (Jup), a component of adherens junctions and desmosomes, was also differently expressed in CME hearts. *Jup*$^{-/-}$ knockout mice display clinical features of arrhythmogenic right ventricular cardiomyopathy (ARVC) [84]. This includes the development of myocardial fibrosis and hypertrophic cardiomyopathy due to a significant loss in desmosomes in *Jup*$^{-/-}$ hearts, both of which are phenotypic features of *Col4a1*$^{+/svc}$ mice. The overlap in signature with the CME dataset is also reflective of the vascular remodelling in our mutant animals which suggests it initiates a molecular response similar to that of coronary occlusion.

We were also interested to explore if there are convergent effects between *Col4a1*$^{+/svc}$ cardiomyopathy and human heart failure, which could highlight a role for the ECM in heart failure. Cross-comparison with DEPs of hypertrophic obstructive cardiomyopathy [85,86] revealed that both displayed changes in the BM components Col4a1, Col4a2 and Col4a6. Furthermore (Myosin heavy chain 6) Myh6, Myosin light chain 4 (Myl4), Actn1, Vinculin (Vcl), Etfdh, Atp2a2, troponin I (TnnI3), Cysteine and glycine-rich protein 3 (Csrp3), Phosphoglucomutase 5 (Pgm5), Acetyl-CoA Acyltransferase 2 (Acaa2), and (2,4 Dienoyl-CoA reductase (Decr1) were all shared- highlighting the relevance of our model and collagen IV in heart pathophysiology with conserved signature involving BM components, sarcomeric proteins, fatty acid beta oxidation and mitochondrial respiration (Fig. 11**B**) [87]. These proteins were also shared in a study of the human heart failure with preserved ejection fraction (HFpEF) [88].

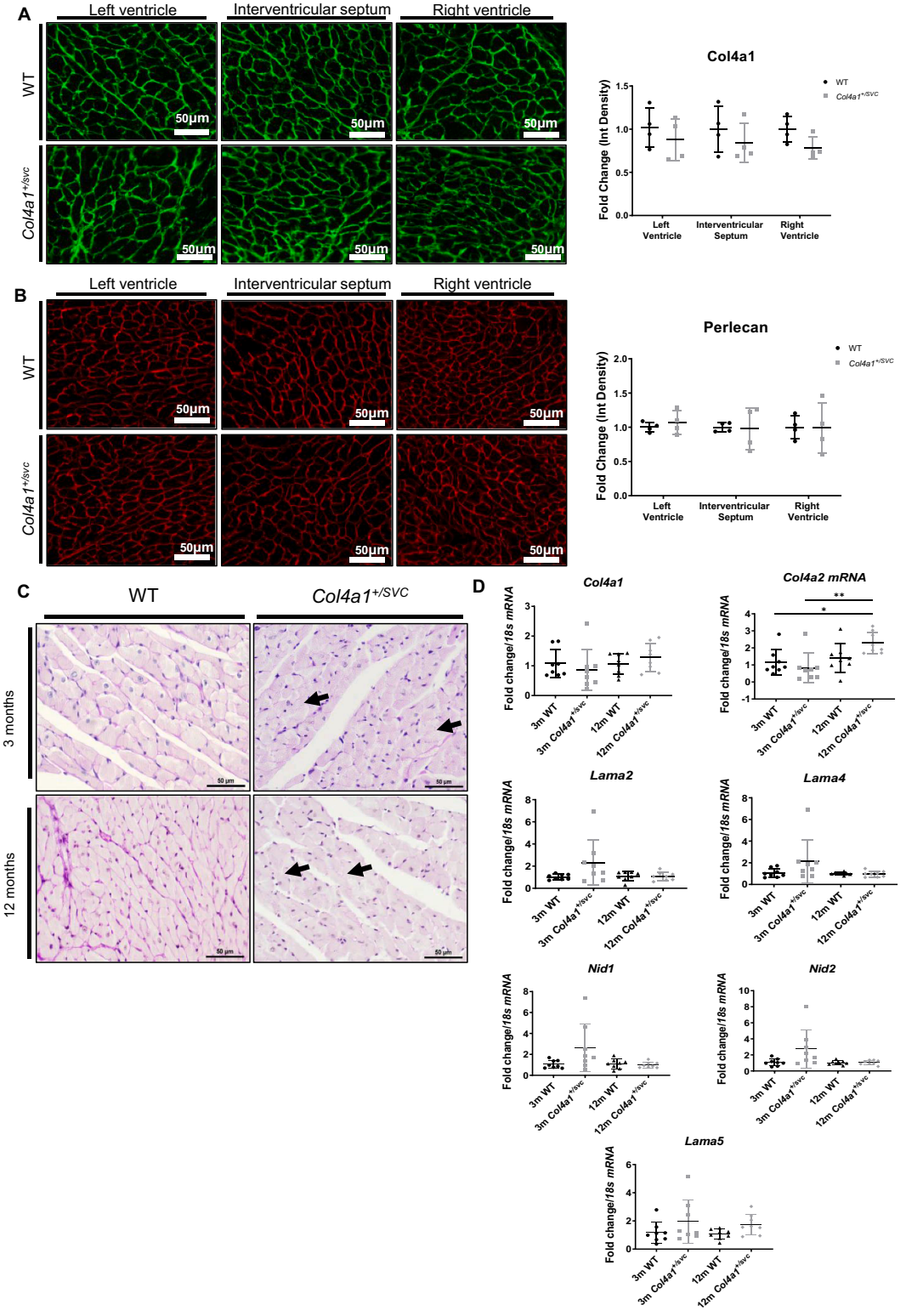


**Fig. 4. Assessing the expression and localisation of key basement membrane components.** Immunohistochemical analysis revealed **(A)** α1(IV) expression was not significantly altered in *Col4a1*$^{+/svc}$ mice α1(IV) (LV $p = 0.4248$ −13.95 %, IVS $p = 0.4000$ −15.79 %, and RV $p = 0.0703$ −21.87 % unpaired two-tailed *t*-tests, WT $n = 4$, *Col4a1*$^{+/svc}$ $n = 4$). (B) Perlecan was also not significantly reduced in *Col4a1*$^{+/svc}$ mice across all regions analysed (LV $p = 0.5031$, IVS $p = 0.9006$, RV $p = 0.9593$ unpaired two-tailed *t*-tests, WT $n = 4$, *Col4a1*$^{+/svc}$ $n = 4$). (C) Periodic acid Schiff staining of left ventricular myocardium in 3 and 12-month-old mice. PAS positive staining (vivid purple) which stains glycoproteins present within the gross basement membrane zone was evident surrounding WT cardiomyocytes and vasculature. At both age points, regions of sparse PAS positive staining were identified in *Col4a1*$^{+/svc}$ hearts (black arrows). qRT-PCR analysis of basement membrane component mRNA expression in 3 and-12-month-old WT and *Col4a1*$^{+/svc}$ hearts. **(D)** *Col4a1, Col4a2, Lama2, Lama4, Lama5, Nid1* and *Nid2* mRNA levels were quantified with no significant difference detected except for Col4a2 ($p = 0.05$ 3-month-old WT vs. 12 m *Col4a1*$^{+/svc}$, $p = 0.0024$ 3-month-old *Col4a1*$^{+/svc}$ vs. 12-month-old *Col4a1*$^{+/svc}$, Kruskal-Wallis with Dunn's multiple comparisons test). Gene expression levels normalised to 18 s mRNA (WT $n = 8$, *Col4a1*$^{+/svc}$ $n = 8$).

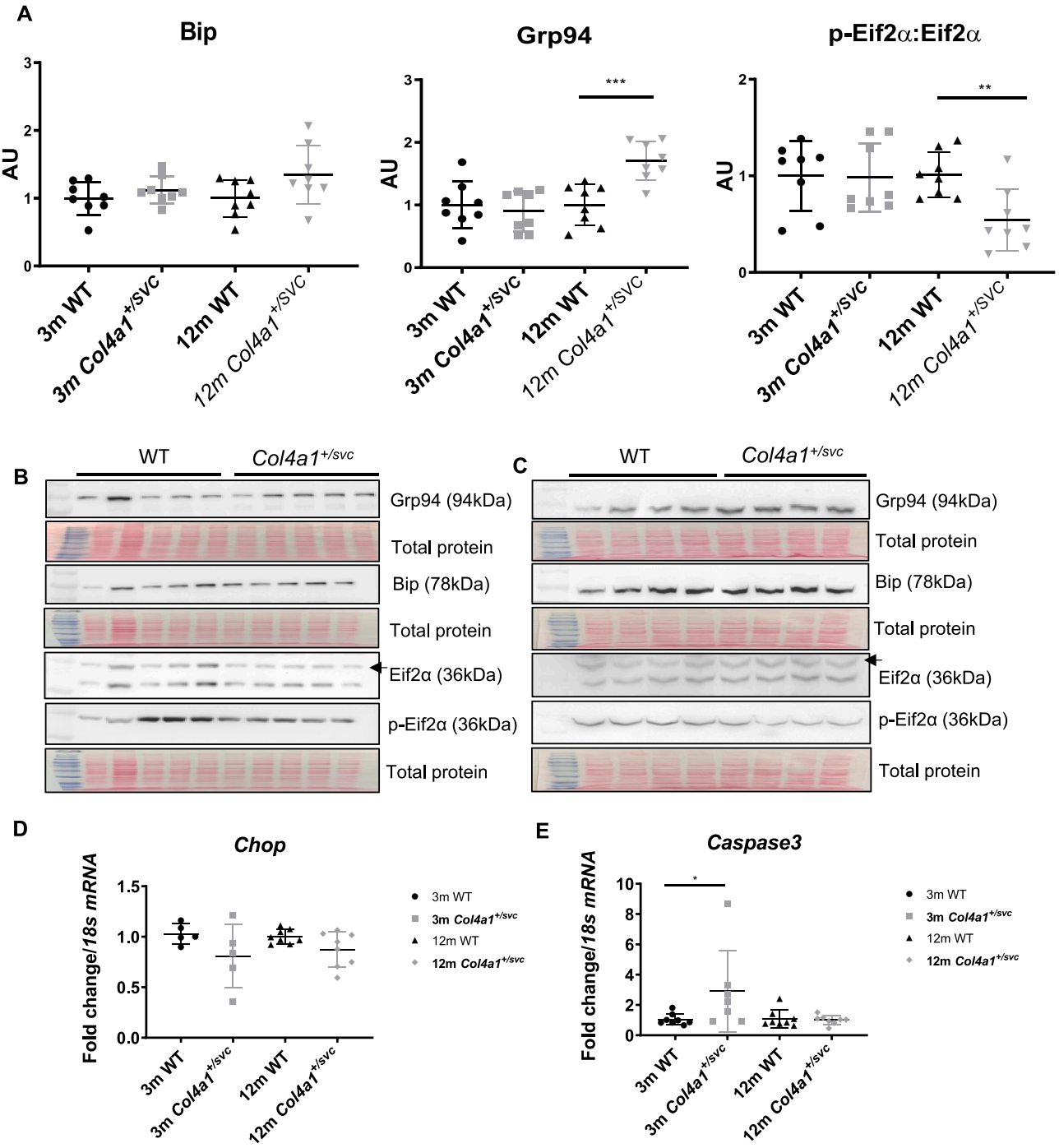


**Fig. 5.** ***Col4a1*$^{+/svc}$ mice display age dependant activation of the unfolded protein response.** **(A)** Quantification of protein levels of key UPR activation markers at 3-months old (Bip $p = 0.2926$, unpaired two-tailed *t*-test. Grp94 $p = 0.7209$, Mann-Whitney U test. p-Eif2α/Eif2α $p = 0.9591$, unpaired two-tailed *t*-test, WT $n = 8$, *Col4a1*$^{+/svc}$ $n = 8$) and12-months-old (Bip $p = 0.0753$, unpaired two-tailed *t*-test), Grp94 ($p = 0.0006$, unpaired two-tailed *t*-test), EIF2α: p-EIF2α ($p = 0.0049$, unpaired two-tailed *t*-test, WT $n = 8$, *Col4a1*$^{+/svc}$ $n = 8$). **(B)** Representative immunoblots of Bip, Grp94, and EIF2α: p-EIF2α in 3-month-old and **(C)** 12-month-old mice. Levels normalised to total protein (ponceau stain). **(D)** Expression of pro-apoptotic gene *Chop* was not significantly altered in 3 or 12-month-old mutant animals ($p = 0.1721$ mean fold change WT = 1.028 *Col4a1*$^{+/svc}$ = 0.8068, two-tailed *t*-test, WT $n = 5$–8, *Col4a1*$^{+/svc}$ $n = 8$). **(E)** *Caspase3* mRNA expression significantly increased in 3-month-old *Col4a1*$^{+/svc}$ mice ($p = 0.0289$ mean fold change WT = 1.049 *Col4a1*$^{+/svc}$ = 2.908, unpaired two-tailed *t*-test, WT $n = 8$, *Col4a1*$^{+/svc}$ $n = 8$). Expression levels normalised to *18 s* mRNA.

## Discussion

### *Cardiac structural and functional phenotypes in Col4a1*$^{+/SVC}$ *mice*

Our investigation of the cardiac aspects of collagen type IV related disease has identified novel cardiac phenotypes and expanded the spectrum of cardiac defects due to *Col4a1* mutations. This is a key new insight as Gould syndrome remains poorly defined, and our data also indicate a potential of age-dependent cardiac failure in patients.

Mutations in *Col4a1* results in hypertrophic response of the right ventricular myocardium and increased size of myocardial clefting of the left ventricular myocardium. The development of tissue and cell type dependent mechanisms within a single organ has been previously characterised by our group for the kidney [37]. The molecular basis of

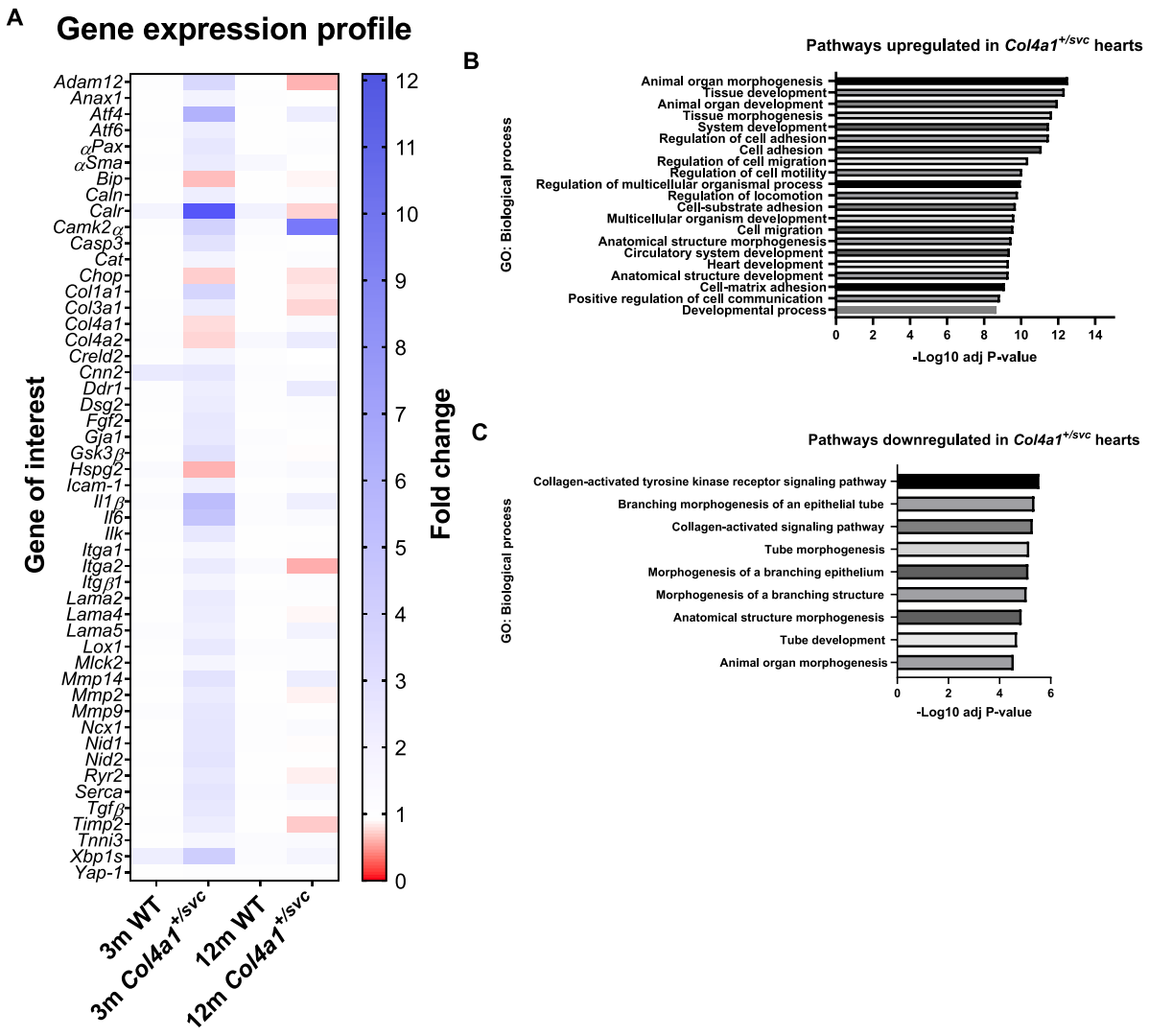


**Fig. 6. Gene expression profile of cardiac candidate genes in *Col4a1*$^{+/svc}$ mice. (A)** Heatmap of the average fold change in mRNA levels of 50 candidate genes indicated proportional to fold change normalised to *18 s* mRNA levels. Upregulated biological processes in 3-month-old Col4a1 mutant hearts. **(B)** GO enrichment for biological processes for upregulated genes expressed in *Col4a1*$^{+/svc}$ hearts. The top 20 pathways identified are shown. **(C)** Downregulated biological processes in 3-month-old Col4a1 mutant hearts. GO enrichment for biological processes for downregulated genes expressed in *Col4a1*$^{+/svc}$ hearts. The top 9 pathways are represented (-Log10 adjusted p-values represented).

these region-specific phenotypes develop remains unclear, but several possibilities exist. Firstly, the development of myocardial fibrosis and hypertrophy within the right ventricular myocardium can be a hallmark of pulmonary disease, specifically pulmonary arterial hypertension [89–92]. Interestingly in this regard is the association of reduced collagen IV levels with pulmonary arterial hypertension and that a different *Col4a1* mutant mouse model has lung defects including reduced alveolarization [93,94]. Additional mechanical strain on the right ventricle due to increased pressures within the pulmonary circulation could trigger maladaptive remodelling of the RV to compensate in a similar fashion to that in *Col4a1*$^{+/svc}$ hearts. The specific temporal relationship between the onset of these phenotypes also remains to be determined.

Our characterisation of the cardiac phenotype in *Col4a1* mutant mice provides further evidence for cell and tissue specific molecular mechanisms of mutations, enhancing our knowledge of how different tissue and cell types respond to the same mutation in a major BM component. In the heart we provide evidence that the disease is underpinned by secretion of mutant protein as opposed to ER stress or collagen IV deficiency [33,35]. In addition, there may also be subtle yet uncharacterised differences in the relative composition of the basement membranes to accommodate the different biomechanical loads the two ventricles experience. Higher levels of collagen IV may be present to cope with the increased demand and as a result a *Col4a1* mutation acting by secreting the mutant protein could lead to phenotypic differences between ventricles. The actual impact of the *Col4a1* mutation on collagen IV network stability and binding to other BM components remains unclear. These could probed using assays which explore dimer and tetramer formation would provide an insight into how glycine missense mutations affect collagen IV network assembly [95].

### *The importance of the basement membrane to key cardiac processes*

Major BM components co-localise with sarcomere landmarks, implying a role in sarcomerogenesis. However, this was only observed in isolated cardiomyocytes [96]. We provide here *in vivo* evidence that the BM is important for cardiomyocyte sarcomere and sarcolemma organisation. BM defects in *Col4a1*$^{+/svc}$ were associated with altered levels of proteins, titin and desmin involved in sarcomere arrangement and assembly. Furthermore, Ehd2 and Trim72, which are involved in sarcolemma stability and repair, were also altered, supporting our hypothesis that the BM contributes to cardiomyocyte sarcolemma stability and

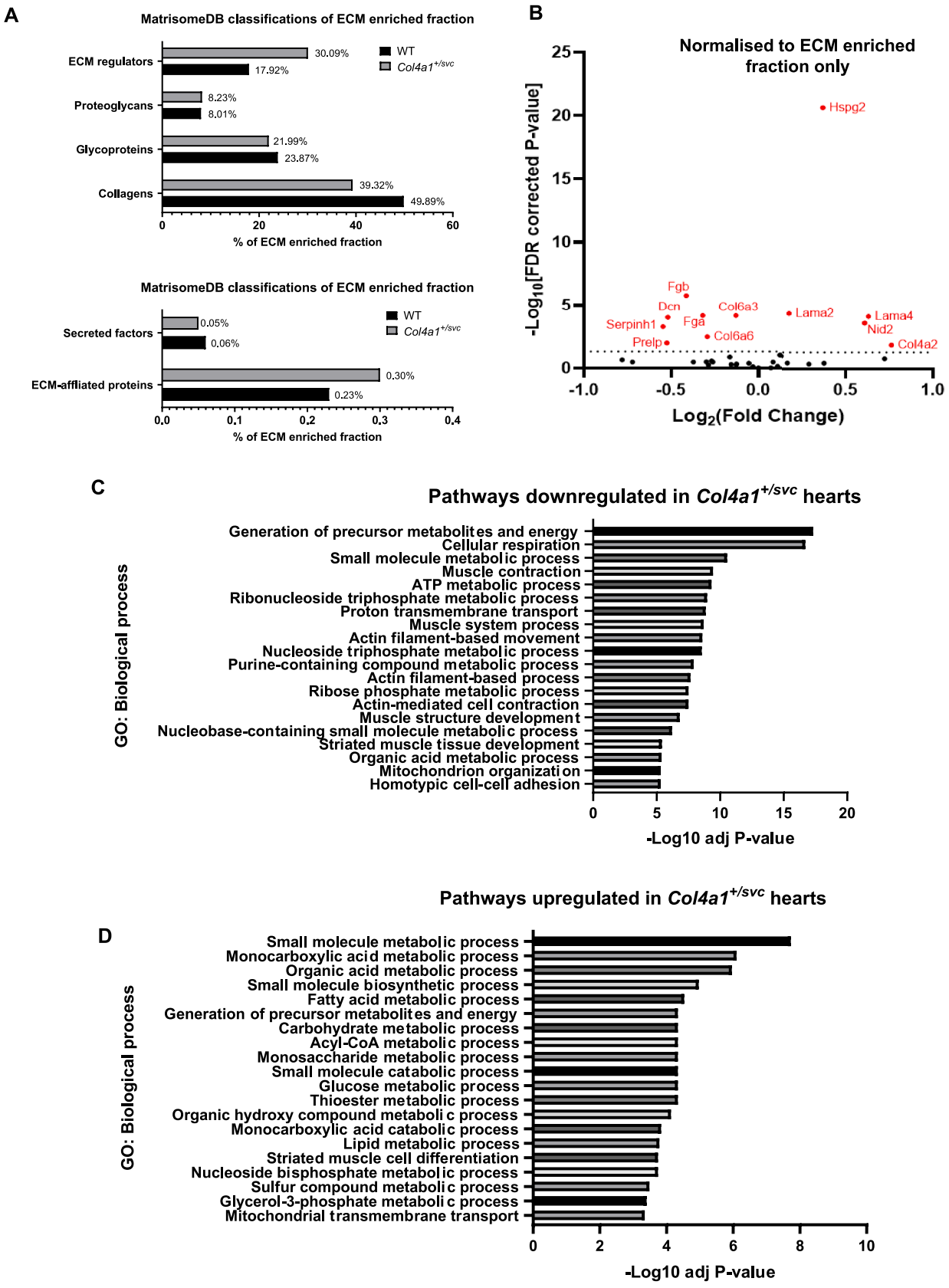


**Fig. 7. Proteomic assessment of ECM enriched cardiac proteins in WT and *Col4a1*$^{+/svc\ hearts}$** **(A)** Composition of matrix enriched fraction base on MatrisomeDB classification of matrix proteins. **(B)** Volcano plots highlight the most significant up and downregulated filtered and normalized to the matrisome. **(C)** GO enrichment for biological processes for proteins significantly upregulated in *Col4a1*$^{+/svc\ hearts}$. The top 20 pathways identified are shown in each case, excluding those judged to be overlapping by Revigo. Downregulated biological processes in 3-month-old Col4a1 mutant hearts. **(D)** GO enrichment for biological processes for proteins significantly downregulated in *Col4a1*$^{+/svc}$ hearts (-Log10 adjusted p-values represented).

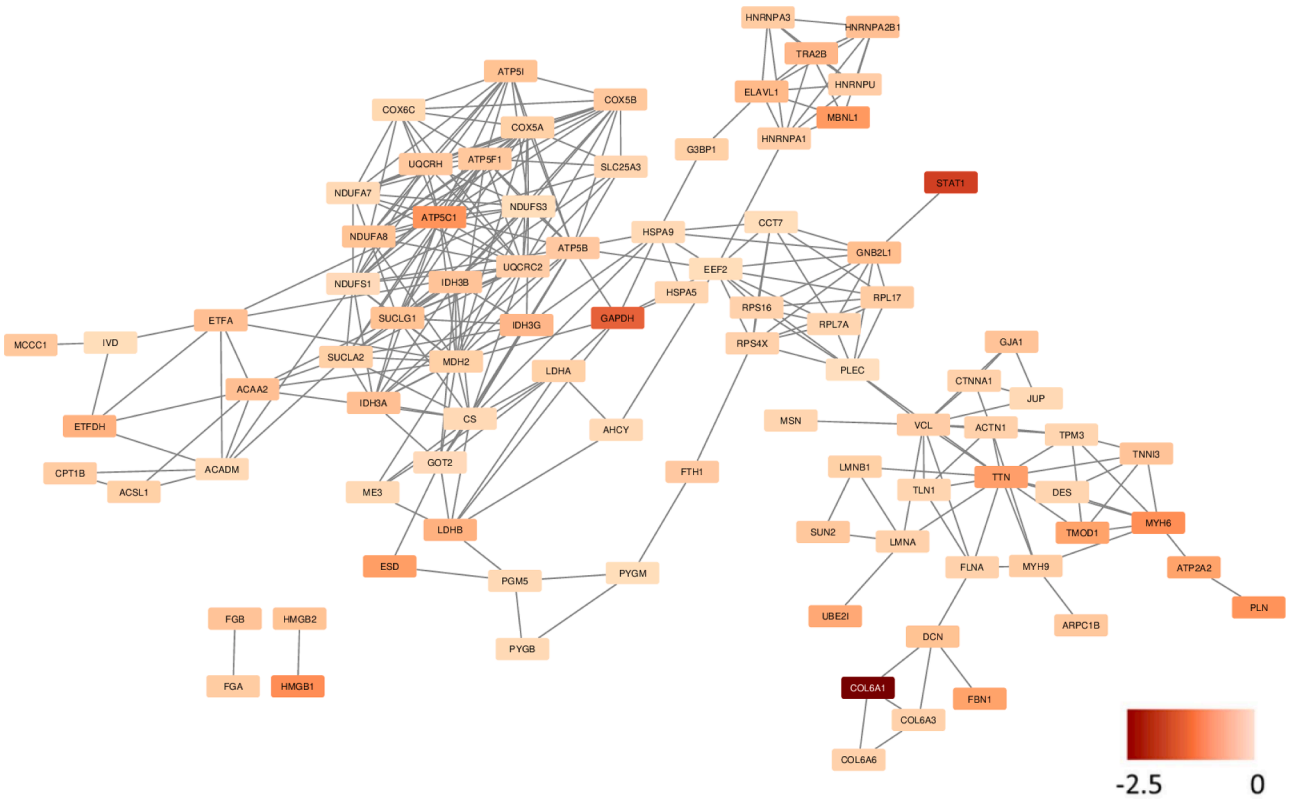


**Fig. 8. Protein interaction networks of significantly downregulated proteins in *Col4a1*$^{+/svc}$ hearts** (proteins identified in both intracellular and extracellular matrix enriched fractions).

maintenance of the microarchitecture necessary for excitation-contraction coupling [3].

It is tempting to suggest a role for altered cardiomyocyte-ECM adhesion and focal adhesion biology caused by compromised BM integrity in this process. While focal adhesion kinase (Fak) levels were not altered, there was downregulation of focal adhesion protein Talin 1, which is recruited by Fak to focal adhesions, and Stat1 which can be activated by Fak to promote cell migration [77,79]. Furthermore, levels of Fhl2, which acts in the cellular response to substrate rigidity by shuttling from the nucleus to binding Fak when the extracellular environment is in a rigid, high-tension state [97], were higher. Given the reduction in myocardial tissue compliance in *Col4a1*$^{+/svc}$ hearts, this could indicate increased interaction between Fhl2 and Fak. Overall, this provides evidence for a mechanism whereby mutant collagen IV in the BM affects the structural support provided by the BM and cell-ECM interaction. This then affects sarcolemma and sarcomere biology and may leave the cardiomyocyte sarcolemma more vulnerable to mechanical injury, which could contribute to the contractile impairment in *Col4a1*$^{+/svc}$ hearts. While this hypothesis requires mechanistic analysis, support comes from recent work demonstrating cardiac dysfunction with fibrosis in *Pomt1*$^{loxP/loxP/M\text{-}CKCre}$ (Pomt1 cKO) mice [98]. The dystroglycan receptors in these matriglycan deficient mice no longer effectively bind their ECM ligands, which caused t-tubules, a cardiac membrane organelle, to become vulnerable to isoprenaline induced cardiac injury [98]. Thus, our data support that BM composition influences the crosstalk between the sarcolemma and ECM for the structural stability of cardiomyocyte microdomains and overall membrane strength.

We also established altered cell metabolic pathways in response to a *Col4a1* mutation, a mechanistic feature likely exacerbates the cardiac functional defects observed. Evidence suggesting a reduced ability to generate ATP was observed through reduced levels of enzymes involved in fatty acid beta oxidation, TCA cycle and mitochondria respiratory chain. This could explain the reduced cardiac function in *Col4a1*$^{+/svc}$ mice. Reduced mitochondrial function resulting in impaired cardiac metabolism is well-documented in cardiovascular disease [98]. However, it remains to be determined whether the metabolic defects are a second primary effect of the mutation or a consequence of other defects as mitochondrial dynamics requires a highly organised sarcomeric network within the cardiomyocytes, a feature which is disrupted in *Col4a1*$^{+/svc}$ hearts. The suggested metabolic shift from fatty acid beta oxidation to glycolysis for ATP generation observed in *Col4a1* mutant mice has previously been observed in hypertrophic cardiomyopathy [99]. This all points towards altered mitochondrial function in response to the cardiac structural defects in *Col4a1*$^{+/svc}$ mice. Alternatively, or in addition, the structural changes including the development of vascular fibrosis and cardiomyocyte hypertrophy coupled with impaired cell-cell and cell-matrix interaction may lead to increased metabolic demand on the heart which is unable to be met. Together, these changes highlight important crosstalk between the BM, mitochondrial dysfunction and adverse metabolic remodelling, a feature commonly observed in heart failure [100].

## Conclusion

These data provide novel insight into the role of BM within cardiac biology and both rare hereditary and common cardiovascular disorders. They highlight that the BM plays a vital role in regulating cardiac contractile function, the onset and progression of fibrosis, and via alteration due to a *Col4a1* mutation, can lead to altered cardiovascular metabolic process. Many patients with *COL4A1* mutations present early in childhood and cardiac assessment has remained under-reported, meaning evidence of a cardiac component has been limited. However, given the age dependent progression observed here, our data support that monitoring of cardiac function as patients age is warranted. Our data also points to potential cardiac manifestations that may occur in Gould

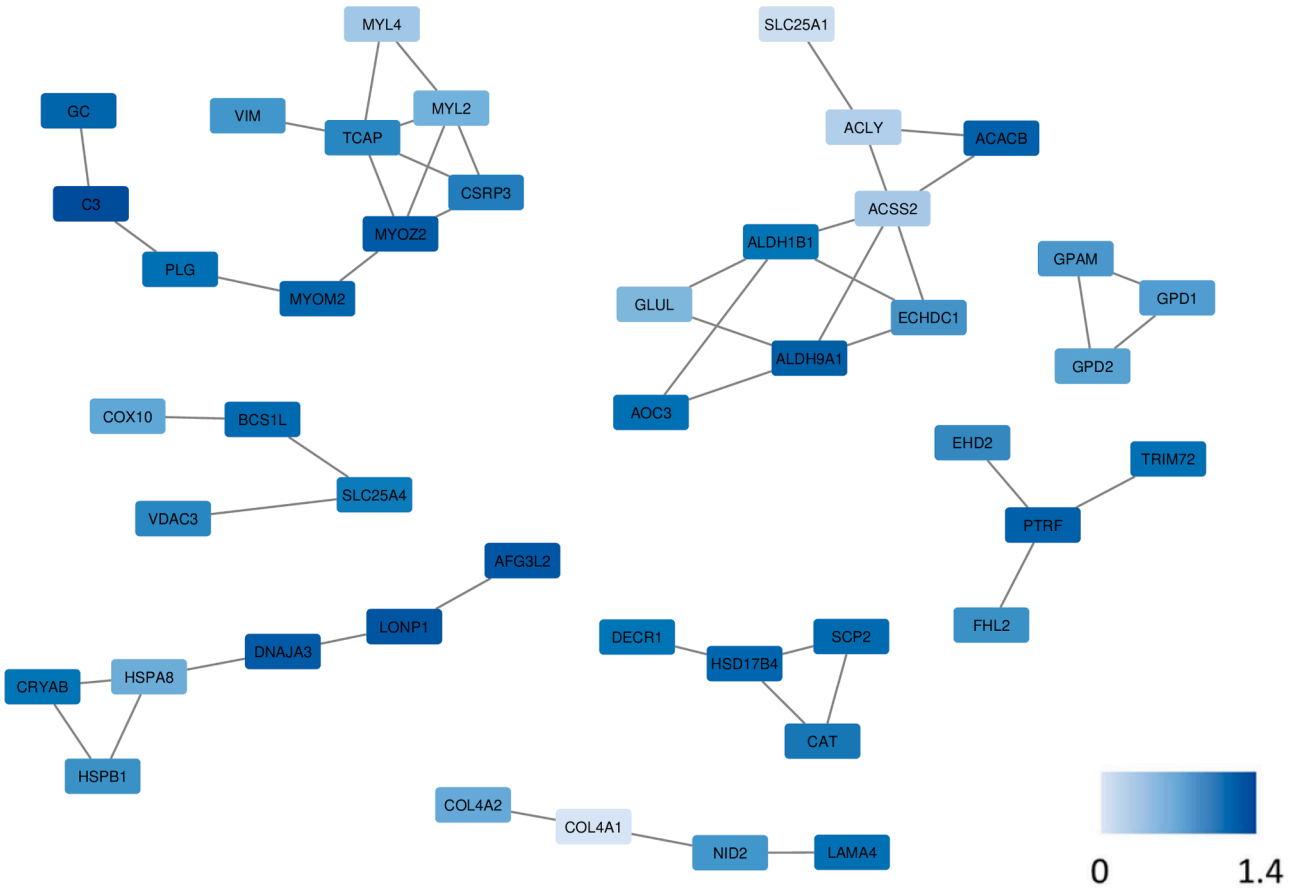


**Fig. 9. Protein interaction networks of significantly upregulated proteins in *Col4a1*$^{+/svc}$ hearts** (proteins identified in both intracellular and extracellular matrix enriched fractions).

Syndrome patients. Furthermore, we previously detected rare coding putative pathogenic *COL4A1/2* variants in a population cohort of intracerebral haemorrhage and small vessel disease [33], and myocardial infarcts were genetically associated with a *COL4A1* variant [101]. Thus, our data raises the hypothesis that genetic COL4 variants may also contribute to some cases of heart disease in the general population. The comparison between our novel cardiac proteome of *Col4a1*$^{+/svc}$ hearts and published proteomics datasets reveal a convergence in proteome changes between various cardiac pathologies in both mouse and human samples, which provides evidence of a potential role of the BM and ECM in some of these cardiac diseases. Finally, our novel mechanistic data presents an unexplored opportunity to target and develop therapeutics focussing on restoration of BM-cardiomyocyte interactions to target collagen IV associated cardiac disease.

## Experimental procedures

### *Animal studies*

All animal work was carried out under UK Home Office project license number 9995833. *Col4a1*$^{+/svc}$ mice harbour a *Col4a1* glycine to aspartic acid mutation (G1064D) [102]. The strain of *Col4a1*$^{+/svc}$ (small with vacuolar cataract) mice used in this study were of a C57/BL6J genetic background with littermate WT mice included as age matched controls. Cohorts consisted of male and female mice, and allocation of animals to cohorts was randomised and researchers were blinded to genotype. All tissues were harvested between 9 am and 12pm to reduce any confounding impact of circadian rhythm.

### *Histology*

Hearts were fixed overnight in 4 % paraformaldehyde, sectioned longitudinally into 1 mm slice with a 4 chambered view using an acrylic sagittal mouse heart slicer matrix (Zivic Labs, Model # HSMA001–2), and paraffin embedded. 5 μm sections were stained using haematoxylin and eosin, periodic acid Schiff and picrosirius red using standard protocols.

### *Immunohistochemistry*

Cryosections for immunohistochemistry were prepared from OCT-embedded 1 mm longitudinal slices frozen on liquid nitrogen as previously described and were sectioned (10 μM) using a Leica CM1520 cryostat [33]. Cryosections were briefly fixed in acetone before antigen retrieval with 0.1 M HCl/KCl for 10 min. Following blocking in phosphate buffered saline 0.1 % Tween (PBST) with 10 % goat serum for 1 hour, sections were incubated overnight at 4 °C with primary antibodies. Following and secondary antibodies (details provided in **supplementary Tables 4.1–4.4**) prior to nuclear staining with Hoechst #33342 2ug/ml (Life technologies - #H3570). Slides were imaged using the Nikon ECLIPSE Ts2-FL microscope and NIS-Elements (Nikon) imaging software. Images were taken of the left ventricle, interventricular septum, and right ventricle. Fluorescence was quantified as corrected integrated density using ImageJ analysis.

### *Langendorff isolated heart preparations*

Mice were euthanized using cervical dislocation and the heart rapidly excised from the level above the thymus and immediately

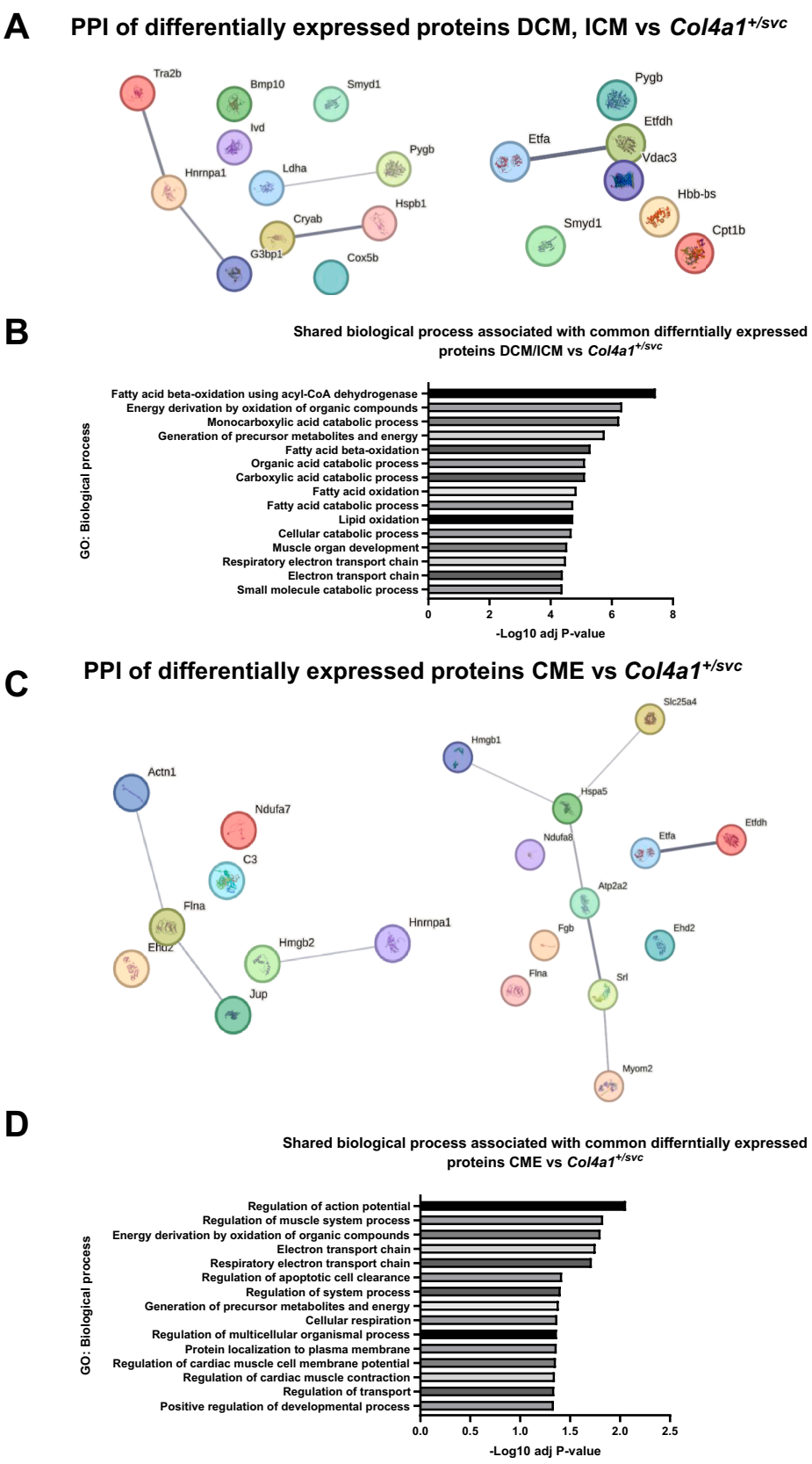


**Fig. 10. Proteomic dataset based on (Lu et al., 2019). (A)** Protein-protein interactions of shared differentially expressed proteins between *Col4a1*$^{+/svc}$, dilated cardiomyopathy and ischaemic cardiomyopathy mapped using STRING v12.0 PPI network mapping platform. **(B)** GO enrichment analysis (*PANTHER*v19.0) for shared biological processes between *Col4a1*$^{+/svc}$, dilated cardiomyopathy and ischaemic cardiomyopathy. **(C) Proteomic dataset based on (Chen et al., 2018).** Protein-protein interactions of shared differentially expressed proteins between *Col4a1*$^{+/svc}$ and coronary microembolism. **(D)** GO enrichment analysis (*PANTHER*v19.0) for shared biological processes between *Col4a1*$^{+/svc}$ and coronary microembolism.

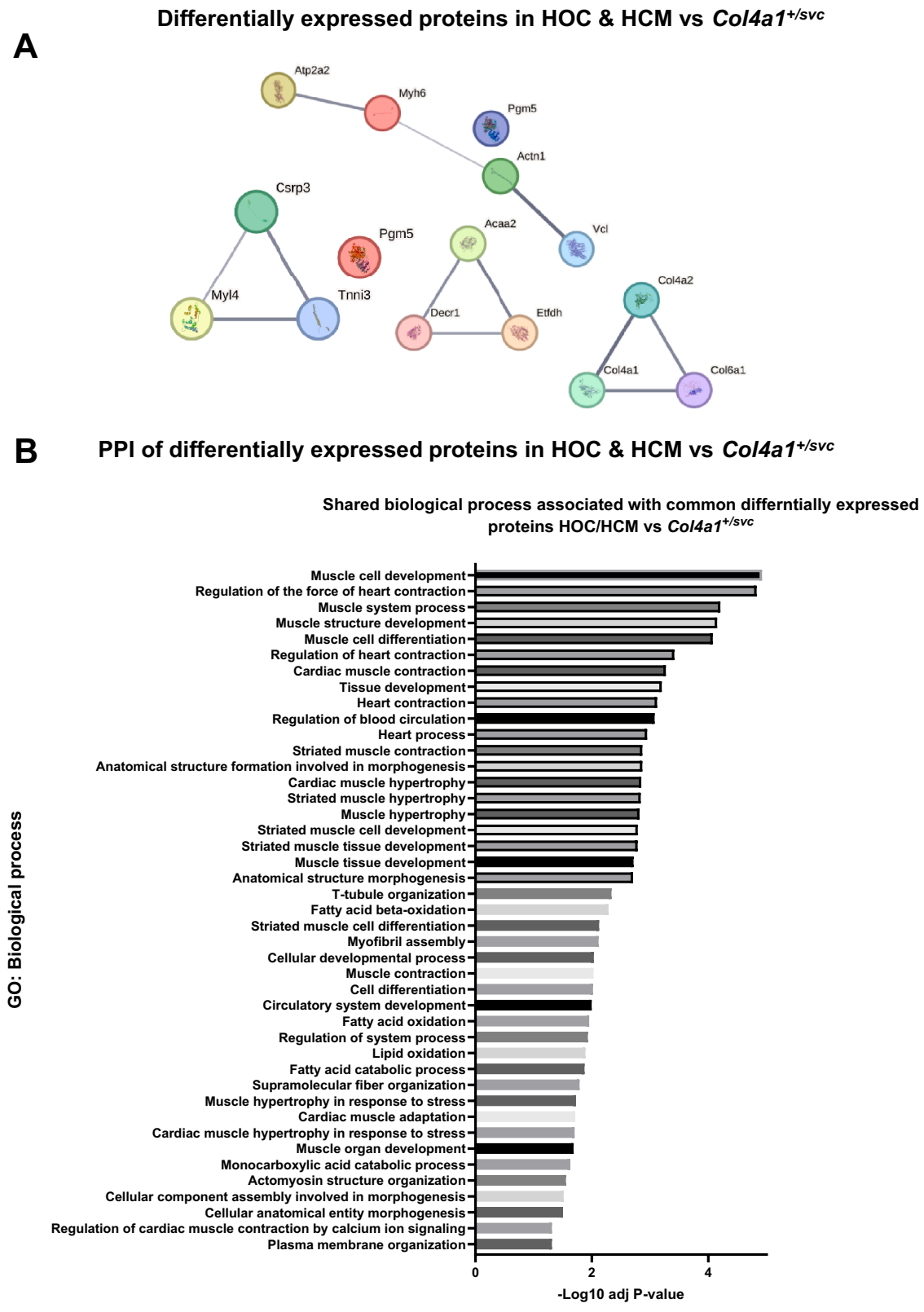


**Fig. 11. Proteomic dataset based on (Coats et al., 2018), (Previs et al., 2022), and (Munoz et al., 2022). (A)** Protein-protein interactions of shared differentially expressed proteins between *Col4a1*$^{+/svc}$, hypertrophic obstructive cardiomyopathy and hypertrophic cardiomyopathy mapped using STRING v12.0 PPI network mapping platform. **(B)** GO enrichment analysis (*PANTHER*v19.0) for shared biological processes between *Col4a1*$^{+/svc}$, dilated cardiomyopathy and ischaemic cardiomyopathy.

arrested in ice cold Tyrode's solution (Composition detailed in **supplementary Table 5**). Isolated hearts were secured to a Langendorff retrograde perfusion apparatus (ADInstruments LTD, UK) and immediately perfused with 37 °C Tyrode's solution which was constantly oxygenated with 95 % oxygen 5 % $CO_2$. The LV pressure balloon was inserted into the left ventricle before inflating to a $P_{min}$ of ~8 mmHg. Recordings were collected and analysed using LabChart data acquisition software. Parameters of cardiac function included Pmin (mmHg), Pmax (mmHg), dP/dtmin (mmHg/s), dP/dtmax (mmHg/s), left ventricular developed pressure (mmHg), coronary flow (mL/min), and heart rate (BPM). Stimulation rates were controlled using right atrial pacing and contractility parameters recorded over a range of frequencies.

*Immunoblotting*

Samples were mixed and heated to 95 °C for 5 min prior to loading on 10 % SDS-PAGE gels. Gels were loaded in Mini-PROTEAN® Tetra Vertical Electrophoresis Cell Tanks (Bio-Rad) with tris-glycine-SDS running buffer (0.25 M glycine, 16.75 mM tris, 0.05 % SDS) and a pre-stained molecular weight ladder (Blue Pre-stained Protein Standard, Broad Range 11–250 kDa P7718, NEB). Proteins were transferred onto 0.2 μm pore nitrocellulose membrane (GE Healthcare) using wet transfer protocol in transfer buffer (24.8 mM tris, 0.67 M glycine, 20 % absolute ethanol) at 350 mA for 90 min. After blocking membranes for 1 hour at room temperature with 1x TBS 0.2 % tween (TBS-T) containing 5 % non-fat dry milk, membranes were incubated with primary antibodies at 4 °C overnight in 5 % non-fat dry milk or 5 % BSA TBS-T for probing of phosphorylated proteins. Following washes (3 × 10 min), blots were incubated with horse radish peroxidase (HRP) conjugated secondary antibodies in 5 % milk TBS-T for 1 hour at room temperature. Protein bands were detected via chemiluminescence using LuminataTM Forte Western HRP Substrate (Merck Millipore) on a Bio-Rad ChemiDoc XRS Gel Documentation System and imaged with Quantity One® 1-D analysis software. Protein loading was corrected using total protein densitometry analysis following ponceau staining (0.5 % ponceau S, 1 % acetic acid). Densitometric analysis of the bands detected and ponceau stains was carried out using ImageJ software.

*Enrichment of extracellular matrix proteins from cardiac protein lysates*

Enrichment of extracellular matrix proteins for proteomic analysis was achieved through adaptation of previously described protocols for ECM enrichment in both kidney and cerebrovascular tissue [103,104]. 100 mg of ventricular tissue was homogenised and resuspended in ice cold TB buffer 10:1 vol to tissue weight (10 mM Tris, 150 mM NaCl, 25 mM EDTA, 1 % (vol/vol) Triton X-100, Roche cOmplete™ EDTA-free Protease Inhibitor Cocktail). Resuspended lysates were centrifuged, and supernatant removed. The pellet was washed with TB buffer (10:1 ratio) before resuspension and decellularisation in ice cold EB buffer (20 mM NH4OH, 0.5 % (vol/vol) Triton-X in PBS) 10:1 vol to tissue weight. The remaining ECM enriched pellets were resuspended in sample buffer (100 mM Tris pH 6.8; 25 % glycerol; 10 % SDS; 10 % beta-mercaptoethanol) in 5:1 vol to tissue weight. Protein samples were stored at −80 °C until further use. Validation of ECM enrichment was established following proteomic analysis of extracellular and intracellular fractions of two wild type samples (**Supplementary figure 4**).

*Mass spectrometry and proteomic analysis*

Dried peptides were resuspended in 10 μL 0.1 % formic acid in 5 % acetonitrile (ACN). Samples were analysed using an ultiMate® 3000 Rapid Separation LC system (RSLC, Dionex Corporation) coupled to first a Orbitrap Elite, for quality control, and then a Q Exactive HF Mass Spectrometer (Thermo Fisher). Peptides were selected by DDA for fragmentation automatically and data was acquired for 90 min in positive mode. Mass spectrometry results files were exported into Proteome Discoverer (PD) for identification and quantification. All searches included the fixed modification for carbamidomethylation on cysteine residues resulting from IAA treatment to prevent cysteine bonding. The variable modifications included in the search were oxidised methionine (monoisotopic mass change, +15.955 Da) and phosphorylation of threonine, serine, and tyrosine (79.966 Da). A maximum of 2 missed cleavages per peptide was allowed. Peptides were searched against the Swissprot database using Sequest HT with a maximum false discovery rate of 1 %.

*Assessment of tissue deformation and elasticity using atomic force microscopy (AFM)*

AFM is a technique utilised to provide micromechanical characterization of a substrate and derivation of the Young's Modulus, a measure of a material's stiffness and its ability to resist deformation [105]. The Young's modulus of 10 μm cryosections of the heart was analysed using a NanoWizard 3 Bioscience AFM (JPK, Berlin, Germany). Nanoindentation measurements were performed at room temperature on sections incubated with PBS containing 1:1000 protease inhibitor cocktail solution (Sigma-Aldrich). Calibration of cantilever sensitivity against a glass slide was performed using 0.3 N/m cantilevers (TL-CONT from Nanosensors) mounted with a 20 μm diameter spherical silica bead using a cantilever approach speed of 2.0 μm/s. The thermal noise method was used to determine spring constant using the JPK SPM software. Nanoindentation measurements were then performed using force mapping mode in 100 × 100 $\mu m^2$, 5 × 5 pixels maps. Young's moduli were calculated using the processing functions of JPK DP software; curves were fitted to no more than 10 % indentation depth to ensure compliance with the Hertz model. Regional mapping information is detailed in supplementary data (**Supplementary figure 2**).

*Gene expression analysis*

Using a 1 mm acrylic coronal heart matrix (Harvard Apparatus UK) a 3 mm portion of the heart at the level of the mid myocardium was collected. Cardiac tissue was homogenised and RNA isolated with 1 ml of TRIzol™ reagent (Invitrogen #15596026). Isolated RNA was treated with DNase (DNA-free™ Kit DNase Treatment and Removal Reagent – Thermofisher AM1906) and RNA concentration was determined using a NanoDrop ND-1000 spectrophotometer. cDNA was synthesized from 1ug of DNase treated RNA using the High-Capacity cDNA Reverse Transcription Kit (Applied Biosystems #4368814). qRT-PCR was carried out using an Applied Biosystems 7900HT Fast Real-Time PCR system. Ct values were corrected to mouse *18S* mRNA. PCR and qRT-PCR cycling conditions and primer information is detailed in supplementary Tables 2.1, 2.2 & 3.

*Comparisons of the $Col4a1^{+/SVC}$ proteome with published cardiac disease datasets*

Published proteomics datasets of both murine and human cardiac pathologies including hypertrophic cardiomyopathy, dilated cardiomyopathy, ischemic cardiomyopathy and coronary microembolism were collated and filtered for differentially expressed proteins (adjusted P value <0.05) [80,82,83,88,106]. These DEPs were then manually cross-referenced with DEPs from our $Col4a1^{+/svc}$ dataset to identify shared significantly up and down-regulated proteins. GO enrichment analysis (*PANTHER*v19.0) for shared biological processes was performed between shared DEPs and mapped using STRING v12.0 PPI network mapping platform.

## Funding

This work was supported by the MRC [MR/R005567/1 (to T.V.A.)]; the BHF [PG/15/92/31813 (to T.V.A.)]; the Stroke Association [grant

number 16VAD_04 (to T.V.A.)]; Heart Research U.K. [grant number RG 2664/17/20 (to T.V.A, F.Q. and E.B)]. M.C acknowledges MRC (MR/S005412)]; and the BBSRC [CASE DTP studentship to A.H.; BB/L024551/1) and Royal Society (RGS/R1/231400).BB/T001984/1 to J. S.).

## Author contributions

EB primary lead in conducting experiments, data analysis and manuscript preparation. A.H and J.S contributed mass spectrometry proteomics and data analysis. M.W, M.C, M.S.S contributed atomic force microscopy experiments. O.R.G & W.F contributed Langendorff perfusion equipment and expertise. E.H, E.M, C.L contributed to cardiac phenotypic assessment. All authors reviewed and contributed to final manuscript preparation. T.V.A, F.Q, G.L.S, and C.L were all involved in project outline and funding co-applicants. T.V.A, F.Q, G.L.S were all involved in data interpretation and presentation. T.V.A principal investigator of project and lead in project concept and experimental approach.

## Declaration of competing interest

All authors declare no conflict of interest.

## Acknowledgements

The authors would like to thank Biological Services and the veterinary team at the University of Glasgow for their contributions to the management of our animal colonies and advice throughout the duration of this study. We would also like to thank the Anatomy Facility at the University of Glasgow for the continuous use of their histological facilities. Thank you to Margaret Mullin and Leandro Lemgruber Soares for their assistance in association with MVLS imaging facilities. Proteomics was performed by the University of Manchester Biological Mass Spectrometry Core Facility (RRID code: SCR_020987).

## Supplementary materials

Supplementary material associated with this article can be found, in the online version, at doi:10.1016/j.matbio.2025.09.003.

## Data availability

Data will be made available on request.

## References

[1] F. Quondamatteo, Assembly, stability and integrity of basement membranes in vivo, Histochem. J. 34 (2002) 369–381, https://doi.org/10.1023/A:1023675619251.
[2] R. Jayadev, D.R. Sherwood, Basement membranes, Curr. Biol. 27 (2017) R207–R211, https://doi.org/10.1016/j.cub.2017.02.006.
[3] E. Boland, F. Quondamatteo, T. Van Agtmael, The role of basement membranes in cardiac biology and disease, Biosci. Rep. 41 (2021), https://doi.org/10.1042/BSR20204185.
[4] T. Van Agtmael, L. Bruckner-Tuderman, Basement membranes and human disease, Cell Tissue Res. 339 (2010) 167–188, https://doi.org/10.1007/s00441-009-0866-y.
[5] J. Khoshnoodi, V. Pedchenko, B.G. Hudson, Mammalian collagen IV, Microsc. Res. Tech. 71 (2008) 357–370, https://doi.org/10.1002/jemt.20564.
[6] T. Van Agtmael, U. Schlötzer-Schrehardt, L. McKie, D.G. Brownstein, A.W. Lee, S. H. Cross, et al., Dominant mutations of Col4a1 result in basement membrane defects which lead to anterior segment dysgenesis and glomerulopathy, Hum. Mol. Genet. 14 (2005) 3161–3168, https://doi.org/10.1093/hmg/ddi348.
[7] A. Gatseva, Y.Y. Sin, G. Brezzo, T. Van Agtmael, Basement membrane collagens and disease mechanisms, Essays Biochem. 63 (2019) 297–312, https://doi.org/10.1042/EBC20180071.
[8] D.S. Kuo, C. Labelle-Dumais, D.B. Gould, Col4a1 and col4a2 mutations and disease: insights into pathogenic mechanisms and potential therapeutic targets, Hum. Mol. Genet. 21 (2012), https://doi.org/10.1093/hmg/dds346.
[9] A. Dean, T. Van Agtmael, Collagen IV-related diseases and therapies, Collagen Superfamily Collagenopathies (2021) 143–197, https://doi.org/10.1007/978-3-030-67592-9_5.
[10] M.E.C. Meuwissen, D.J.J. Halley, L.S. Smit, M.H. Lequin, J.M. Cobben, R. De Coo, et al., The expanding phenotype of COL4A1 and COL4A2 mutations: clinical data on 13 newly identified families and a review of the literature, Genet. Med. 17 (2015) 843–853, https://doi.org/10.1038/gim.2014.210.
[11] S. Zagaglia, C. Selch, J.R. Nisevic, D. Mei, Z. Michalak, L. Hernandez-Hernandez, et al., Neurologic phenotypes associated with COL4A1/2 mutations: expanding the spectrum of disease, Neurology 91 (2018) e2078–e2088, https://doi.org/10.1212/WNL.0000000000006567.
[12] D.B. Gould, F.C. Phalan, G.J. Breedveld, S.E. van Mil, R.S. Smith, J.C. Schimenti, et al., Mutations in Col4a1 cause perinatal cerebral hemorrhage and porencephaly, Science 308 (2005) 1167–1171, https://doi.org/10.1126/science.1109418.
[13] T. Van Agtmael, U. Schlötzer-Schrehardt, L. McKie, D.G. Brownstein, A.W. Lee, S. H. Cross, et al., Dominant mutations of Col4a1 result in basement membrane defects which lead to anterior segment dysgenesis and glomerulopathy, Hum. Mol. Genet. 14 (2005) 3161–3168, https://doi.org/10.1093/hmg/ddi348.
[14] E. Plaisier, O. Gribouval, S. Alamowitch, B. Mougenot, C. Prost, M.C. Verpont, et al., COL4A1 mutations and hereditary angiopathy, nephropathy, aneurysms, and muscle cramps, N. Engl. J. Med. 357 (2007) 2687–2695, https://doi.org/10.1056/NEJMoa071906.
[15] K. Vahedi, S. Alamowitch, Clinical spectrum of type IV collagen (COL4A1) mutations: a novel genetic multisystem disease, Curr. Opin. Neurol. 24 (2011) 63–68, https://doi.org/10.1097/WCO.0b013e32834232c6.
[16] Y.C. Weng, A. Sonni, C. Labelle-Dumais, M. De Leau, W.B. Kauffman, M. Jeanne, et al., COL4A1 mutations in patients with sporadic late-onset intracerebral hemorrhage, Ann. Neurol. 71 (2012) 470–477, https://doi.org/10.1002/ana.22682.
[17] M. Jeanne, D.B. Gould, Genotype-phenotype correlations in pathology caused by collagen type IV alpha 1 and 2 mutations, Matrix Biol. 57–58 (2017) 29–44, https://doi.org/10.1016/j.matbio.2016.10.003.
[18] M. Jeanne, J. Jorgensen, D.B. Gould, Molecular and genetic analyses of collagen type IV mutant mouse models of spontaneous intracerebral hemorrhage identify mechanisms for stroke prevention, Circulation 131 (2015) 1555–1565, https://doi.org/10.1161/CIRCULATIONAHA.114.013395.
[19] A. Nichols, B.J. Sánchez-Sánchez, S. Marcotti, M.-C. Díaz-de-la-Loza, L. C. Menezes, T. Wang, et al., Drosophila Col4a1 Glycine mutations highlight allelic heterogeneity and mechanistic pleiotropy, Matrix Biol. 140 (2025) 113–122, https://doi.org/10.1016/j.matbio.2025.07.005.
[20] San Parkin J Des, J.D. Antonio, V. Pedchenko, B. Hudson, S.T. Jensen, J. Savige, Mapping structural landmarks, ligand binding sites, and missense mutations to the collagen IV heterotrimers predicts major functional domains, novel interactions, and variation in phenotypes in inherited diseases affecting basement membranes, Hum. Mutat. 32 (2011) 127–143, https://doi.org/10.1002/humu.21401.
[21] S. Okano, S. Shimada, R. Tanaka, A. Okayama, A. Kajihama, N. Suzuki, et al., Life-threatening muscle complications of COL4A1-related disorder, Brain Dev. 42 (2020) 93–97, https://doi.org/10.1016/j.braindev.2019.09.001.
[22] H. Patel, M. Elkhwad, G.C. Martin, Central nervous system and cardiac abnormalities in the setting of a De novo heterozygous Col4a1 variant, Am. J. Case Rep. 24 (2023), https://doi.org/10.12659/AJCR.938651.
[23] E. Plaisier, O. Gribouval, S. Alamowitch, B. Mougenot, C. Prost, M.C. Verpont, et al., *COL4A1* mutations and hereditary angiopathy, nephropathy, aneurysms, and muscle cramps, N. Engl. J. Med. 357 (2007) 2687–2695, https://doi.org/10.1056/NEJMoa071906.
[24] H. Hutchinson, L. Brinkley, J. Philip, W. Barras, M. Bleiweis, J. Jacobs, et al., 907: SUCCESSFUL ORTHOTOPIC-HEART TRANSPLANT (OHT) IN AN INFANT WITH COL4A1 MUTATION, Crit. Care Med. 53 (2025), https://doi.org/10.1097/01.ccm.0001102292.64136.6d.
[25] Y.P. Wang, D.J. Wang, Niu Z Bin, W.T Cui, Chromosome 13q deletion syndrome involving 13q31-qter: a case report, Mol. Med. Rep. 15 (2017) 3658–3664, https://doi.org/10.3892/mmr.2017.6425.
[26] C.J. Mcmahon, C. Breathnach, D.R. Betts, F.H. Sharkey, M.T. Greally, De Novo interstitial deletion 13q33.3q34 in a male patient with double outlet right ventricle, microcephaly, dysmorphic craniofacial findings, and motor and developmental delay, Am. J. Med. Genet. a 167 (2015) 1134–1141, https://doi.org/10.1002/ajmg.a.36978.
[27] W. Yang, F.L. Ng, K. Chan, X. Pu, R.N. Poston, M. Ren, et al., Coronary-heart-disease-associated genetic variant at the COL4A1/COL4A2 locus affects COL4A1/COL4A2 expression, vascular cell survival, atherosclerotic plaque stability and risk of myocardial infarction, PLoS Genet. 12 (2016), https://doi.org/10.1371/journal.pgen.1006127.
[28] K. Rannikmäe, G. Davies, P.A. Thomson, S. Bevan, W.J. Devan, G.J. Falcone, et al., Common variation in COL4A1/COL4A2 is associated with sporadic cerebral small vessel disease, Neurology 84 (2015) 918–926, https://doi.org/10.1212/WNL.0000000000001309.
[29] K.V. Tarasov, S. Sanna, A. Scuteri, J.B. Strait, M. Orrù, A. Parsa, et al., COL4A1 is associated with arterial stiffness by genome-wide association scan, Circ. Cardiovasc. Genet. 2 (2009) 151–158, https://doi.org/10.1161/CIRCGENETICS.108.823245.
[30] T.N. Turley, J.L. Theis, J.M. Evans, Z.C. Fogarty, R. Gulati, S.N. Hayes, et al., Identification of rare genetic variants in familial spontaneous coronary artery dissection and evidence for shared biological pathways, J. Cardiovasc. Dev. Dis. 10 (2023) 393, https://doi.org/10.3390/jcdd10090393.

[31] M. Uemura, N. Tanaka, S. Ando, T. Yanagihara, O. Onodera, Missense variants in COL4A1/2 are associated with cerebral aneurysms: a case report and literature review, Neurol. Int. 16 (2024) 226–238, https://doi.org/10.3390/neurolint16010015.
[32] X. Peng, Y. Li, N. Liu, S. Xia, X. Li, Y. Lai, et al., Plasma proteomic insights for identification of novel predictors and potential drug targets in atrial fibrillation: a prospective cohort study and mendelian randomization analysis, Circ. Arrhythm. Electrophysiol. 17 (2024), https://doi.org/10.1161/CIRCEP.124.013037.
[33] S. McNeilly, C.R. Thomson, L. Gonzalez-Trueba, Y.Y. Sin, A. Granata, G. Hamilton, et al., Collagen IV deficiency causes hypertrophic remodeling and endothelium-dependent hyperpolarization in small vessel disease with intracerebral hemorrhage, EBioMedicine 107 (2024) 105315, https://doi.org/10.1016/j.ebiom.2024.105315.
[34] F.E. Jones, L.S. Murray, S. McNeilly, A. Dean, A. Aman, Y. Lu, et al., 4-Sodium phenyl butyric acid has both efficacy and counter-indicative effects in the treatment of Col4a1 disease, Hum. Mol. Genet. 28 (2019) 628–638, https://doi.org/10.1093/hmg/ddy369.
[35] F.E. Jones, M.A. Bailey, L.S. Murray, Y. Lu, S. McNeilly, U. Schlötzer-Schrehardt, et al., ER stress and basement membrane defects combine to cause glomerular and tubular renal disease resulting from Col4a1 mutations in mice, Dis. Model. Mech. 9 (2016) 165–176, https://doi.org/10.1242/dmm.021741.
[36] T. Van Agtmael, M.A. Bailey, U. Schlötzer-Schrehardt, E. Craigie, I.J. Jackson, D. G. Brownstein, et al., Col4a1 mutation in mice causes defects in vascular function and low blood pressure associated with reduced red blood cell volume, Hum. Mol. Genet. 19 (2010) 1119–1128, https://doi.org/10.1093/hmg/ddp584.
[37] F.E. Jones, M.A. Bailey, L.S. Murray, Y. Lu, S. McNeilly, U. Schlötzer-Schrehardt, et al., ER stress and basement membrane defects combine to cause glomerular and tubular renal disease resulting from Col4a1 mutations in mice, Dis. Model. Mech. 9 (2016) 165–176, https://doi.org/10.1242/dmm.021741.
[38] L.S. Murray, Y. Lu, A. Taggart, N.V. van Regemorter, C. Vilain, M. Abramowicz, et al., Chemical chaperone treatment reduces intracellular accumulation of mutant collagen IV and ameliorates the cellular phenotype of a COL4A2 mutation that causes haemorrhagic stroke, Hum. Mol. Genet. 23 (2014) 283–292, https://doi.org/10.1093/hmg/ddt418.
[39] L.S. Murray, Y. Lu, A. Taggart, N.V. van Regemorter, C. Vilain, M. Abramowicz, et al., Chemical chaperone treatment reduces intracellular accumulation of mutant collagen IV and ameliorates the cellular phenotype of a COL4A2 mutation that causes haemorrhagic stroke, Hum. Mol. Genet. 23 (2014) 283–292, https://doi.org/10.1093/hmg/ddt418.
[40] T. Van Agtmael, U. Schlötzer-Schrehardt, L. McKie, D.G. Brownstein, A.W. Lee, S. H. Cross, et al., Dominant mutations of Col4a1 result in basement membrane defects which lead to anterior segment dysgenesis and glomerulopathy, Hum. Mol. Genet. 14 (2005) 3161–3168, https://doi.org/10.1093/hmg/ddi348.
[41] L.F. Reissig, A.N. Herdina, J. Rose, B.M. Gesek, J.L. Lane, F. Prin, et al., The Col4a2em1(IMPC)Wtsi mouse line: lessons from the deciphering the mechanisms of developmental disorders program, Biol. Open 8 (2019), https://doi.org/10.1242/bio.042895.
[42] S. Israeli-Rosenberg, A.M. Manso, H. Okada, R.S. Ross, Integrins and integrin-associated proteins in the cardiac myocyte, Circ. Res. 114 (2014) 572–586, https://doi.org/10.1161/CIRCRESAHA.114.301275.
[43] C. Chen, R. Li, R.S. Ross, A.M. Manso, Integrins and integrin-related proteins in cardiac fibrosis, J. Mol. Cell Cardiol. 93 (2016) 162–174, https://doi.org/10.1016/j.yjmcc.2015.11.010.
[44] D.E. Michele, Z. Kabaeva, S.L. Davis, R.M. Weiss, K.P. Campbell, Dystroglycan matrix receptor function in cardiac myocytes is important for limiting activity-induced myocardial damage, Circ. Res. 105 (2009) 984–993, https://doi.org/10.1161/CIRCRESAHA.109.199489.
[45] Z. Kabaeva, K.E. Meekhof, Michele DE, Sarcolemma instability during mechanical activity in large myd cardiac myocytes with loss of dystroglycan extracellular matrix receptor function, Hum. Mol. Genet. 20 (2011) 3346–3355, https://doi.org/10.1093/hmg/ddr240.
[46] R.T. Cowling, S.J. Yeo, I.J. Kim, J Il Park, Y. Gu, N.D. Dalton, et al., Discoidin domain receptor 2 germline gene deletion leads to altered heart structure and function in the mouse, Am. J. Physiol. Heart. Circ. Physiol. 307 (2014) H773–H781, https://doi.org/10.1152/ajpheart.00142.2014.
[47] B. Leitinger, Discoidin domain receptor functions in physiological and pathological conditions, Int. Rev. Cell Mol. Biol. 310 (2014) 39–87, https://doi.org/10.1016/B978-0-12-800180-6.00002-5. Elsevier Inc.
[48] D. Hilfiker-Kleiner, U. Landmesser, H. Drexler, Molecular mechanisms in heart failure: focus on cardiac hypertrophy, inflammation, angiogenesis, and apoptosis, J. Am. Coll. Cardiol. 48 (2006) A56–A66, https://doi.org/10.1016/J.JACC.2006.07.007.
[49] D. Borin, I. Pecorari, B. Pena, O. Sbaizero, Novel insights into cardiomyocytes provided by atomic force microscopy, Semin. Cell Dev. Biol. 73 (2018) 4–12, https://doi.org/10.1016/j.semcdb.2017.07.003.
[50] J.C. Benech, G. Romanelli, Atomic force microscopy indentation for nanomechanical characterization of live pathological cardiovascular/heart tissue and cells, Micron 158 (2022) 103287, https://doi.org/10.1016/j.micron.2022.103287.
[51] B. Peña, M. Adbel-Hafiz, M. Cavasin, L. Mestroni, O. Sbaizero, Atomic Force Microscopy (AFM) Applications in Arrhythmogenic Cardiomyopathy, Int. J. Mol. Sci. 23 (2022) 3700, https://doi.org/10.3390/ijms23073700.
[52] E. Verdura, D. Hervé, F. Bergametti, C. Jacquet, T. Morvan, C. Prieto-Morin, et al., Disruption of a miR-29 binding site leading to COL4A1 upregulation causes pontine autosomal dominant microangiopathy with leukoencephalopathy, Ann. Neurol. 80 (2016) 741–753, https://doi.org/10.1002/ana.24782.
[53] M. Jeanne, D.B. Gould, Genotype-phenotype correlations in pathology caused by collagen type IV alpha 1 and 2 mutations, Matrix Biol. 57–58 (2017) 29–44, https://doi.org/10.1016/j.matbio.2016.10.003.
[54] L.S. Murray, Y. Lu, A. Taggart, N.V. van Regemorter, C. Vilain, M. Abramowicz, et al., Chemical chaperone treatment reduces intracellular accumulation of mutant collagen IV and ameliorates the cellular phenotype of a COL4A2 mutation that causes haemorrhagic stroke, Hum. Mol. Genet. 23 (2014) 283–292, https://doi.org/10.1093/hmg/ddt418.
[55] M.J. Randles, F. Lausecker, Q. Kong, H. Suleiman, G. Reid, M. Kolatsi-Joannou, et al., Identification of an altered matrix signature in kidney aging and disease, J. Am. Soc. Nephrol. 32 (2021) 1713–1732, https://doi.org/10.1681/ASN.2020101442.
[56] A.J. Isabella, S. Horne-Badovinac, Dynamic regulation of basement membrane protein levels promotes egg chamber elongation in Drosophila, Dev. Biol. 406 (2015) 212–221, https://doi.org/10.1016/j.ydbio.2015.08.018.
[57] M.H. Rajpar, B. McDermott, L. Kung, R. Eardley, L. Knowles, M. Heeran, et al., Targeted Induction of Endoplasmic Reticulum Stress Induces Cartilage Pathology, PLoS. Genet. 5 (2009) e1000691, https://doi.org/10.1371/journal.pgen.1000691.
[58] R. Omar, M.A. Lee, L. Gonzalez-Trueba, C.R. Thomson, U. Hansen, S. Lianos, et al., The chemical chaperone 4-phenylbutyric acid rescues molecular cell defects of COL3A1 mutations that cause vascular Ehlers Danlos Syndrome, Cell Death. Discov. 11 (2025) 200, https://doi.org/10.1038/s41420-025-02476-y.
[59] R. Gioia, F. Tonelli, I. Ceppi, M. Biggiogera, S. Leikin, S. Fisher, et al., The chaperone activity of 4PBA ameliorates the skeletal phenotype of Chihuahua, a zebrafish model for dominant osteogenesis imperfecta, Hum. Mol. Genet. 26 (2017) 2897–2911, https://doi.org/10.1093/hmg/ddx171.
[60] A. Gatseva, Y.Y. Sin, G. Brezzo, T. Van Agtmael, Basement membrane collagens and disease mechanisms, Essays Biochem. 63 (2019) 297–312, https://doi.org/10.1042/EBC20180071.
[61] M. Al-Thani, M. Goodwin-Trotman, S. Bell, K. Patel, L.K. Fleming, C. Vilain, et al., A novel human iPSC model of COL4A1/A2 small vessel disease unveils a key pathogenic role of matrix metalloproteinases, Stem Cell Rep. 18 (2023) 2386–2399, https://doi.org/10.1016/j.stemcr.2023.10.014.
[62] X. Shao, C.D. Gomez, N. Kapoor, J.M. Considine, C. Grams, Y (Tom) Gao, et al., MatrisomeDB 2.0: 2023 updates to the ECM-protein knowledge database, Nucleic. Acids. Res. 51 (2023) D1519–D1530, https://doi.org/10.1093/nar/gkac1009.
[63] Z. Wang, D.J. Stuckey, C.E. Murdoch, P. Camelliti, G.Y.H. Lip, M. Griffin, Cardiac fibrosis can be attenuated by blocking the activity of transglutaminase 2 using a selective small-molecule inhibitor, Cell Death. Dis. 9 (2018) 613, https://doi.org/10.1038/s41419-018-0573-2.
[64] S. Chen, J. Ma, J. Chi, B. Zhang, X. Zheng, J. Chen, et al., Roles and potential clinical implications of tissue transglutaminase in cardiovascular diseases, Pharmacol. Res. 177 (2022) 106085, https://doi.org/10.1016/j.phrs.2022.106085.
[65] X.W. Cheng, G.-P. Shi, M. Kuzuya, T. Sasaki, K. Okumura, T. Murohara, Role for cysteine protease cathepsins in heart disease, Circulation 125 (2012) 1551–1562, https://doi.org/10.1161/CIRCULATIONAHA.111.066712.
[66] Z. Cai, S. Xu, C. Liu, Cathepsin B in cardiovascular disease: underlying mechanisms and therapeutic strategies, J. Cell Mol. Med. 28 (2024), https://doi.org/10.1111/jcmm.70064.
[67] C.D. Merkel, Y. Li, Q. Raza, D.B. Stolz, A.V. Kwiatkowski, Vinculin anchors contractile actin to the cardiomyocyte adherens junction, Mol. Biol. Cell 30 (2019) 2639–2650, https://doi.org/10.1091/mbc.E19-04-0216.
[68] A.E. Zemljic-Harpf, J. Godoy, O. Platoshyn, E.K. Asfaw, A.R. Busija, A. A. Domenighetti, et al., Vinculin directly binds zonula occludens-1 and is essential for stabilizing connexin 43 containing gap junctions in cardiac Myocytes, J. Cell Sci. (2014), https://doi.org/10.1242/jcs.143743.
[69] C.Y. X'avia Chan, D. Wang, M. Cadeiras, M.C. Deng, P. Ping, S-nitrosylation of TRIM72 mends the broken heart: a molecular modifier-mediated cardioprotection, J. Mol. Cell Cardiol. 72 (2014) 292–295, https://doi.org/10.1016/j.yjmcc.2014.04.004.
[70] C.M. Loescher, A.J. Hobbach, W.A. Linke, Titin (TTN): from molecule to modifications, mechanics, and medical significance, Cardiovasc. Res. (2021), https://doi.org/10.1093/cvr/cvab328.
[71] S.R. Singh, J. Robbins, Desmin and cardiac disease, Circ. Res. 122 (2018) 1324–1326, https://doi.org/10.1161/CIRCRESAHA.118.312965.
[72] M. Mavroidis, Y. Capetanaki, Extensive induction of important mediators of fibrosis and dystrophic calcification in desmin-deficient cardiomyopathy, Am. J. Pathol. 160 (2002) 943–952, https://doi.org/10.1016/S0002-9440(10)64916-4.
[73] D.J. Milner, G.E. Taffet, X. Wang, T. Pham, T. Tamura, C. Hartley, et al., The absence of desmin leads to cardiomyocyte hypertrophy and cardiac dilation with compromised systolic function, J. Mol. Cell Cardiol. 31 (1999) 2063–2076, https://doi.org/10.1006/jmcc.1999.1037.
[74] A. Stephanou, D.S. Latchman, STAT-1: a novel regulator of apoptosis, Int. J. Exp. Pathol. 84 (2003) 239–244, https://doi.org/10.1111/j.0959-9673.2003.00363.x.
[75] C. Zhen, H. Liu, L. Gao, Y. Tong, C. He, Signal transducer and transcriptional activation 1 protects against pressure overload-induced cardiac hypertrophy, FASEB J. 35 (2021), https://doi.org/10.1096/fj.202000325RRR.
[76] J. Le Coq, I. Acebrón, B. Rodrigo Martin, P. López Navajas, D. Lietha, New insights into FAK structure and function in focal adhesions, J. Cell Sci. 135 (2022), https://doi.org/10.1242/jcs.259089.
[77] B. Xie, J. Zhao, M. Kitagawa, J. Durbin, J.A. Madri, J.-L. Guan, et al., Focal adhesion kinase activates stat1 in integrin-mediated cell migration and adhesion,

J. Biol. Chem. 276 (2001) 19512–19523, https://doi.org/10.1074/jbc.M009063200.
[78] X. Peng, Inactivation of focal adhesion kinase in cardiomyocytes promotes eccentric cardiac hypertrophy and fibrosis in mice, J. Clin. Investig. 116 (2005) 217–227, https://doi.org/10.1172/JCI24497.
[79] C. Lawson, S.-T. Lim, S. Uryu, X.L. Chen, D.A. Calderwood, D.D. Schlaepfer, FAK promotes recruitment of talin to nascent adhesions to control cell motility, J. Cell Biol. 196 (2012) 223–232, https://doi.org/10.1083/jcb.201108078.
[80] A. Chen, Z. Chen, Y. Xia, D. Lu, J. Jia, K. Hu, et al., Proteomics analysis of myocardial tissues in a mouse model of coronary microembolization, Front. Physiol. 9 (2018), https://doi.org/10.3389/fphys.2018.01318.
[81] D. Lu, Y. Xia, Z. Chen, A. Chen, Y. Wu, J. Jia, et al., Cardiac proteome profiling in ischemic and dilated cardiomyopathy mouse models, Front. Physiol. 10 (2019), https://doi.org/10.3389/fphys.2019.00750.
[82] C.J. Coats, W.E. Heywood, A. Virasami, N. Ashrafi, P. Syrris, C. dos Remedios, et al., Proteomic analysis of the myocardium in hypertrophic obstructive cardiomyopathy, Circ. Genom. Precis. Med. 11 (2018), https://doi.org/10.1161/CIRCGEN.117.001974.
[83] M.J. Previs, T.S. O'Leary, M.P. Morley, B.M. Palmer, M. LeWinter, J.M. Yob, et al., Defects in the proteome and metabolome in human hypertrophic cardiomyopathy, Circ. Heart. Fail. 15 (2022), https://doi.org/10.1161/CIRCHEARTFAILURE.121.009521.
[84] D. Li, Y. Liu, M. Maruyama, W. Zhu, H. Chen, W. Zhang, et al., Restrictive loss of plakoglobin in cardiomyocytes leads to arrhythmogenic cardiomyopathy, Hum. Mol. Genet. 20 (2011) 4582–4596, https://doi.org/10.1093/hmg/ddr392.
[85] C.J. Coats, W.E. Heywood, A. Virasami, N. Ashrafi, P. Syrris, C. dos Remedios, et al., Proteomic analysis of the myocardium in hypertrophic obstructive cardiomyopathy, Circ. Genom. Precis. Med. 11 (2018), https://doi.org/10.1161/CIRCGEN.117.001974.
[86] M.J. Previs, T.S. O'Leary, M.P. Morley, B.M. Palmer, M. LeWinter, J.M. Yob, et al., Defects in the proteome and metabolome in human hypertrophic cardiomyopathy, Circ. Heart. Fail. 15 (2022), https://doi.org/10.1161/CIRCHEARTFAILURE.121.009521.
[87] M. Valero-Muñoz, E.L. Saw, R.M. Hekman, B.C. Blum, Z. Hourani, H. Granzier, et al., Proteomic and phosphoproteomic profiling in heart failure with preserved ejection fraction (HFpEF), Front. Cardiovasc. Med. 9 (2022), https://doi.org/10.3389/fcvm.2022.966968.
[88] M. Valero-Muñoz, E.L. Saw, R.M. Hekman, B.C. Blum, Z. Hourani, H. Granzier, et al., Proteomic and phosphoproteomic profiling in heart failure with preserved ejection fraction (HFpEF), Front. Cardiovasc. Med. 9 (2022), https://doi.org/10.3389/fcvm.2022.966968.
[89] M. Arrigo, L.C. Huber, S. Winnik, F. Mikulicic, F. Guidetti, M. Frank, et al., Right ventricular failure: pathophysiology, diagnosis and treatment, Card. Fail. Rev. 5 (2019) 140–146, https://doi.org/10.15420/cfr.2019.15.2.
[90] J. Gomez-Arroyo, L.E. Santos-Martinez, A. Aranda, T. Pulido, M. Beltran, L. Muñoz-Castellanos, et al., Differences in right ventricular remodeling secondary to pressure overload in patients with pulmonary hypertension, Am. J. Respir. Crit. Care Med. 189 (2014) 603–606, https://doi.org/10.1164/rccm.201309-1711LE.
[91] S. Rain, M.L. Handoko, P. Trip, C.T.-J. Gan, N. Westerhof, G.J. Stienen, et al., Right ventricular diastolic impairment in patients with pulmonary arterial hypertension, Circulation 128 (2013) 2016–2025, https://doi.org/10.1161/CIRCULATIONAHA.113.001873.
[92] A. Llucià-Valldeperas, F.S. de Man, H.J. Bogaard, Adaptation and maladaptation of the right ventricle in pulmonary vascular diseases, Clin. Chest Med. 42 (2021) 179–194, https://doi.org/10.1016/j.ccm.2020.11.010.
[93] C.J. Rhodes, H. Im, A. Cao, J.K. Hennigs, L. Wang, S. Sa, et al., RNA sequencing analysis detection of a novel pathway of endothelial dysfunction in pulmonary arterial hypertension, Am. J. Respir. Crit. Care Med. 192 (2015) 356–366, https://doi.org/10.1164/rccm.201408-1528OC.
[94] M. Loscertales, F. Nicolaou, M. Jeanne, M. Longoni, D.B. Gould, Y. Sun, et al., Type IV collagen drives alveolar epithelial–endothelial association and the morphogenetic movements of septation, BMC Biol. 14 (2016) 59, https://doi.org/10.1186/s12915-016-0281-2.
[95] E.N. Pokidysheva, S.F. Tufa, D.R. Keene, B.G. Hudson, S.P. Boudko, Targeted incorporation of collagen IV to the basement membrane: a step forward for developing extracellular protein therapies, J. Biol. Chem. 301 (2025) 110384, https://doi.org/10.1016/j.jbc.2025.110384.
[96] H. Yang, T.K. Borg, H. Liu, B.Z. Gao, Interactive relationship between basement-membrane development and sarcomerogenesis in single cardiomyocytes, Exp. Cell Res. 330 (2015) 222–232, https://doi.org/10.1016/j.yexcr.2014.08.020.
[97] N. Nakazawa, A.R. Sathe, G.V. Shivashankar, M.P. Sheetz, Matrix mechanics controls FHL2 movement to the nucleus to activate p21 expression, Proc. Natl. Acad. Sci. 113 (2016), https://doi.org/10.1073/pnas.1608210113.
[98] J.M. Hord, M.E. Anderson, S.J. Prouty, S. Melton, Z. Gastel, K. Zimmerman, et al., Matriglycan maintains t-tubule structural integrity in cardiac muscle, Proc. Natl. Acad. Sci. 121 (2024), https://doi.org/10.1073/pnas.2402890121.
[99] M.F. Allard, B.O. Schonekess, S.L. Henning, D.R. English, G.D. Lopaschuk, Contribution of oxidative metabolism and glycolysis to ATP production in hypertrophied hearts, Am. J. Physiol.-Heart Circ. Physiol. 267 (1994) H742–H750, https://doi.org/10.1152/ajpheart.1994.267.2.H742.
[100] T. Doenst, T.D. Nguyen, E.D. Abel, Cardiac metabolism in heart failure, Circ. Res. 113 (2013) 709–724, https://doi.org/10.1161/CIRCRESAHA.113.300376.
[101] W. Yang, F.L. Ng, K. Chan, X. Pu, R.N. Poston, M. Ren, et al., Coronary-heart-disease-associated genetic variant at the COL4A1/COL4A2 locus affects COL4A1/COL4A2 expression, vascular cell survival, atherosclerotic plaque stability and risk of myocardial infarction, PLoS. Genet. 12 (2016) e1006127, https://doi.org/10.1371/journal.pgen.1006127.
[102] C. Thaung, Novel ENU-induced eye mutations in the mouse: models for human eye disease, Hum. Mol. Genet. 11 (2002) 755–767, https://doi.org/10.1093/hmg/11.7.755.
[103] R. Lennon, A. Byron, J.D. Humphries, M.J. Randles, A. Carisey, S. Murphy, et al., Global analysis reveals the complexity of the human glomerular extracellular matrix, J. Am. Soc. Nephrol. 25 (2014) 939–951, https://doi.org/10.1681/ASN.2013030233.
[104] J. Barallobre-Barreiro, F. Baig, M. Fava, X. Yin, M. Mayr, Glycoproteomics of the extracellular matrix: a method for intact glycopeptide analysis using mass spectrometry, J. Vis. Exp. (2017), https://doi.org/10.3791/55674.
[105] S. Liu, Y. Han, L. Kong, G. Wang, Z. Ye, Atomic force microscopy in disease-related studies: exploring tissue and cell mechanics, Microsc. Res. Tech. 87 (2024) 660–684, https://doi.org/10.1002/jemt.24471.
[106] D. Lu, Y. Xia, Z. Chen, A. Chen, Y. Wu, J. Jia, et al., Cardiac proteome profiling in ischemic and dilated cardiomyopathy mouse models, Front. Physiol. 10 (2019), https://doi.org/10.3389/fphys.2019.00750.